ANL-79-109

ANL-79-109

CHEMICAL ENGINEERING DIVISION

FUEL CYCLE PROGRAMS
QUARTERLY PROGRESS REPORT

July—September 1979

by

M. J. Steindler, R. A. Couture, K. F. Flynn,
L. J. Jardine, W. J. Mecham, R. H. Pelto,
M. G. Seitz, and Jacqueline Williams

ARGONNE NATIONAL LABORATORY, ARGONNE, ILLINOIS

Prepared for the U. S. DEPARTMENT OF ENERGY
under Contract W-31-109-Eng-38

TABLE OF CONTENTS

	Page
ABSTRACT	1
SUMMARY	1
I. METAL ENCAPSULATION OF RADIOACTIVE WASTE IN METAL	4
A. Determination of the Leach Rates for Nuclear Waste Materials	4
1. Introduction	
2. Experimental Results	5
3. Conclusions	16
B. Characterization of Impact Fracture of Brittle Solid-Waste Forms	16
1. Introduction	16
2. Deformation of Brittle Materials by Mechanical Impact	17
3. The Lognormal Particle-Size Distribution	17
4. Application of the Energy and Size Relationships to Impact Testing	19
5. Conclusions	24
II. TRANSPORT PROPERTIES OF NUCLEAR WASTE IN GEOLOGIC MEDIA	25
A. Introduction	25
B. Experimental	26
1. Porosity Determination From Densities	26
2. Porosity of Particulate Basalt Based on Intergranular Volume Measurements	27
3. Porosity of Particulate Basalt Based on Elution of Tritiated Water	28
C. Cesium and Rubidium Adsorption by Limestone in a Radiation Field	28
D. Apparatus Development	34
III. TRACE-ELEMENT TRANSPORT IN LITHIC MATERIAL BY FLUID FLOW AT HIGH TEMPERATURE	37
A. Introduction	37
B. Theory: Anion Sorption on Oxides and Clay Minerals	37
1. pH Dependence	37
2. Steric Hindrance and the Shape of the Isotherm	38
C. Determination of the Iodate Sorption Isotherm at Trace Concentrations	40
1. Experimental Procedures	40
2. Results	41

TABLE OF CONTENTS (contd)

	Page
D. Sorption of Iodate by Pelagic Red Clay and Hematite from Seawater	42
1. Experimental Procedures	42
2. Results	43
E. Sorption of HOI by Kaolinite or Aluminum Oxide	44
F. Sorption of Iodate and Selenite from Solutions - Test of the Models	44
G. Disposal of Iodine-129	45
REFERENCES	47

LIST OF FIGURES

No.	Title	Page
1.	Effect of Temperature on Leach Rate	10
2.	Leach Rates for Cesium from PNL-Glass	15
3.	Results of Measurements of the Fracture Surface Energy, γ_s, of Pyrex and Quartz at Various Specimen Net Impact Energy Densities for Compression Tests, Single Impact Tests and Multiple Impact Tests	18
4.	Cumulative Lognormal Plot of Measured Particle Size Distributions for Various Impact Tests of Glass Materials	19
5.	Lognormal Plots of Data Reported for Three Types of Impacted Glass Compositions at Four Energy Densities	22
6.	Lognormal Plot of Data Reported for Impacted Glass Specimens Receiving the Same Total Energy but with a Different Number of Impacts	23
7.	Schematic Diagram used in Identifying Locations on a Test Tube Rack in a Radiation Field	30
8.	Cesium Partition Coefficients for Several Concentrations of Cesium or Rubidium	31
9.	Rock-Column Holder with Pressurized Teflon Jacket	34
10.	Apparatus to be used in Leach-Migration Experiments with Solidified Waste Containing Plutonium, Americium, and Neptunium	35
11.	Sorption of Iodate by Hematite	42
12.	Selenite Sorption by FeOOH	45

LIST OF TABLES

No.	Title	Page
1.	Activation Products in Potential Nuclear Waste Materials	5
2.	Sequential Incremental 25°C Leach Rates in Quiescent Water for Various Materials Associated with Nuclear High-Level-Waste Studies	7
3.	Activated Species from High-Energy Neutron Activation of Metals	9
4.	Leach Rates for Metals Using Saturated WIPP Brine as Leachant	9
5.	Leach Rates for PNL 76-68 Glass at Indicated Temperatures	11
6.	Sequential Leach Rates for (76-68) PNL-Glass (Uranium-Spiked) in 25°C Distilled Water	12
7.	Sequential Leach Rates for (76-68) PNL-Glass (Uranium-Spiked) in Distilled Water	13
8.	Sequential Leach Rates for 76-68 PNL Glass (Plutonium-Spiked) in Distilled Water	14
9.	Selected Test Data on Impact Fracture of Brittle Specimens	20
10.	Lognormal Parameters of Impact Fracture of Three Different Glass Compositions	23
11.	Bulk Density of Granulated Basalt Measured in 1.0-cm-ID Tubes	26
12.	Bulk Density of Granulated Basalt Measured in 1.3-cm-ID Tubes	27
13.	Porosity of 20-50 Mesh Sentinel Gap Basalt Based on Tritiated Water Elution	29
14.	Dose Rates at Locations Specified in Fig. 12	30
15.	Partition Coefficients for Rubidium and Cesium from Bath Tests with Irradiated and Nonirradiated Samples	32
16.	Compositions of Buffer Solutions	41
17.	Isotherm for Adsorption of Iodate by Fe_2O_3, Showing Probable Errors	41
18.	Sorption of Iodate by Red Clay and Hematite in Seawater and Modified Seawater	43
19.	Sorption of Iodate by Hematite	46

CHEMICAL ENGINEERING DIVISION

FUEL CYCLE PROGRAMS
QUARTERLY PROGRESS REPORT

July—September 1979

by

M. J. Steindler, R. A. Couture, K. F. Flynn,
L. J. Jardine, W. J. Mecham, R. H. Pelto,
M. G. Seitz, and Jacqueline Williams

ABSTRACT

In a project to identify the advantages and disadvantages of encapsulating solidified waste forms in a metal matrix, leach rates of hazardous radionuclides from various matrix materials as a function of temperature are being studied. Also, a methodology for analyzing particle size distributions obtained in impact-testing of brittle waste-form materials has been applied to the impact testing of Pyrex spheres and to earlier impact tests of a variety of materials.

The transport properties of nuclear waste in geologic media are being studied. Porosity of basalt columns was measured by a method based on the elution of tritiated water. Batch tests were performed to determine the effect of rubidium concentration on cesium adsorption by limestone. An apparatus for infiltrating intact rocks with high-pressure groundwater solutions was constructed.

In work on trace-element transport in lithic material, the sorption by Fe_2O_3 of iodate in concentrations of 10^{-2} to 10^{-13} M and from pH 3 to 8.7 was measured, as was the sorption of iodate by sea sediments.

SUMMARY

Metal Encapsulation of Radioactive Waste in Metal

Determination of the Leach Rates for Nuclear Waste Materials. The leaching characteristics of potential nuclear waste materials, including metals (both metal matrix and canister materials) and solid waste substances (*e.g.*, glass, SYNROC, calcine, etc.), are being studied using a neutron activation technique. The TRIGA reactor at the University of Illinois at Champaign-Urbana is being used as an alternative activation source to the decommissioned ANL CP-5 reactor.

How the variables associated with a leaching medium affect the leach rates of specific hazardous radionuclides from waste glasses (*e.g.*, PNL borosilicate glass formulation 76-68) is being considered. Of the variables, temperature has been shown to have the most pronounced effect. Leach rates as

a function of temperature are reported for a dozen elements. Cesium leach rate is particularly sensitive to temperature, increasing by four orders of magnitude as the temperature increases from 20°C to 290°C. Time sequential leach tests at each of the temperatures studied, lasting about 60 days, indicate a slow decrease in leach rate with time. This phenomenon is commonly observed in leach studies and is attributed to the effects of diffusion in the solid phase.

Characterization of Impact Fracture of Brittle Solid-Waste Forms. A method of analyzing particle size distributions obtained in impact testing of brittle waste form materials is summarized. The methodology includes (1) a linear two-parameter lognormal correlation of the weight fraction smaller than any given particle size, (2) a mathematical function of the two lognormal parameters to determine the total surface area in terms of a dimensionless shape factor, and (3) a surface energy constant to predict the anticipated increase of surface area from the known energy absorbed by impact of the brittle material. Preliminary measurements were made on impacted glass specimens. The results, as well as reanalyzed impact test data reported by others, are used as examples of the methodology.

Transport Properties of Nuclear Waste in Geologic Media

Work this quarter consisted of (1) porosity measurements of a rock column of the type used in infiltration experiments and (2) batch tests to determine the effect of rubidium concentration on cesium adsorption by limestone. Also described is experimental apparatus used to confine a solid rock core in a fluid stream under high pressure for study of leach migration characteristics of radionuclides. The apparatus is used to infiltrate intact rock cores of low porosity with groundwater solutions at high pressure.

The porosity of a single granulated rock column varied. Possibly, air entrapped in the column was responsible for the different porosities measured.

Results of batch tests indicate that trace concentrations of rubidium in groundwater solution greatly decrease the adsorption of cesium on limestone. Rubidium concentration has nearly the same effect on cesium adsorption as does cesium concentration in groundwater on cesium adsorption. Because rubidium is thirty times more abundant in nature than is cesium, rubidium in groundwater is more likely than cesium to control the extent of sorption of radiocesium from groundwater by rock.

Trace-Element Transport in Lithic Material by Fluid Flow at High Temperature

Experimental and theoretical study of adsorption of iodine species and selenite ions from aqueous solutions by ferric oxides at another site has been reported. Sorption of IO_3^- by Fe_2O_3 was determined as a function of iodate concentration from 10^{-13} to 10^{-2} M and from pH 3 to 8.7.

Sorption of potential-determining anions such as iodate is thought to take place mainly by replacement of surface hydroxyl groups, according to

$$\equiv OH + IO_3^- = \equiv OIO_2 + OH^-$$

Because OH^- ions are produced by the reaction, the reaction is strongly favored by acid solutions. On the other hand, sorption of a weak acid, such as HOI (pK_a = 10), should show a maximum amount adsorbed at about the pH of zero point of charge of the oxide surface. For aluminum and iron oxides, this is in the neutral to slightly alkaline range, corresponding to the pH of many natural waters.

The amount of anion sorbed was derived as a function of its dissolved concentration. It was assumed that each sorbed anion sterically covers more than one sorption site, so that a cluster of x free sites is required for sorption of an anion. From this assumption, the following isotherm is derived:

$$\frac{\Gamma/\kappa}{(1 - \Gamma/\kappa)^x} = K(pH)c$$

where Γ = amount sorbed, κ = anion sorption capacity, c = dissolved concentration of the sorbed ion, and K(pH) = equilibrium constant. Previous data for sorption of selenite ions by FeOOH fit this equation very well, with x = 5.2, showing that the model is valid for some cases. However, the iodate data do not fit the model. Two possible reasons are (1) binding of iodate in the interphase region of the double layer and (2) sorption at more than one type of sorption site.

As a practical conclusion from this work, two possible methods of disposal of ^{129}I are suggested. First is burial as IO_3^- in pelagic red clay, which may have enough capacity to sorb an appreciable fraction of the IO_3^-. Second, it is suggested that since coal may sorb I^- strongly, coal might be used as backfill around a repository.

I. METAL ENCAPSULATION OF RADIOACTIVE WASTE IN METAL

(L. J. Jardine, K. Flynn, W. Mecham and R. Pelto)

The major objective of this program is to identify the advantages and disadvantages of encapsulating solidified radioactive waste forms in a metal matrix. The net attributes of metal encapsulation, if any, are to be identified by comparisons of waste form properties and fabrication methods with those of other well-developed solidification alternatives, *i.e.*, calcination and vitrification in the special case of high-level radioactive wastes. Laboratory-scale investigations are in progress specifically aimed at generating data required to further assess likely or unresolved problem areas.

A study aimed at assessing the impact resistance of metal-encapsulated (brittle) waste forms in comparison to glass waste forms has continued during this period. Experimental studies have continued to focus upon the determination of leach rates and of the impact resistance of simulated waste forms.

A. Determination of the Leach Rates for Nuclear Waste Materials

(K. Flynn)

1. Introduction

Any transport of hazardous radionuclides from waste to the biosphere depends, among other things, on the rate at which these radionuclides are transferred from a solid phase to a mobile aqueous phase. This transfer phenomenon is commonly called leaching.

Radioactive waste will be incorporated into an inert solid matrix surrounded by one or more barriers to the environment. For the purposes of containment, the rate of penetration of the barrier material (*e.g.*, canister) is of prime concern since the penetration of the canister material allows the aqueous phase to contact the waste matrix. When aqueous contact is made the rate of dissolution of the specific hazardous radionuclides (*e.g.*, ^{137}Cs, ^{90}Sr, ^{99}Tc, ^{239}Pu, etc) becomes of prime concern.

Measurements related to the penetration by corrosion and/or leaching of canister barrier materials, the leach-rate of waste-form matrix materials, and the dissolution of specific hazardous radionuclides are discussed in this report.

A neutron activation analysis (NAA) technique has been employed. The details of this technique, together with a critique of its advantages and disadvantages, were reported previously [FLYNN]. Operation of the ANL Research Reactor having been terminated, alternative irradiation facilities have been selected for these studies. The TRIGA reactor at the University of Illinois at Champaign-Urbana has been established to be a suitable facility. A similar reactor at the University of Wisconsin in Madison has been confirmed as a backup facility if it becomes necessary to use it.

Several samples have been shipped to Champaign, irradiated in the TRIGA reactor, and returned to ANL via commercial carrier. A 300-lb pot used for shipment is large enough to accommodate any envisaged irradiation samples.

The time lapses associated with cooling and shipment were considered tolerable for our purposes. Should experiments with short-lived activities ever become desirable, it is possible to reduce these time lapses to less than 6 h by providing our own carrier.

Variables associated with the leaching medium are being considered in these studies. Among these variables, temperature seems to have the most pronounced effect. In order to study this effect precisely, controlled-temperature equipment has been secured. A constant-temperature bath has been installed to make measurements in the range from slightly above ambient to about 90°C. About twenty samples can be measured simultaneously. Primary containers of polypropylene will be used in these studies. In addition, high-pressure autoclaves for studying leach rates at elevated temperatures (*i.e.*, up to 300°C) have been in use for some time [STEINDLER-1979B].

2. Experimental Results

Studies are being pursued of the leaching characteristics of potential nuclear waste materials, including metals (both metal-matrix and canister materials) and solid waste substances (*e.g.*, glass, SYNROC, calcine, etc.). The pertinent activation products present after neutron irradiation in many of the matrix and canister materials under investigation are listed in Table 1. The activity of each activation product is included to allow comparision. These activities are based on the element concentrations in the materials irradiated and the irradiation conditions chosen (*i.e.*, 24-h irradiation at a neutron flux of 6×10^{12} n/cm^2·s). Those species with the highest activities have the greatest potential for making measurements of leach rates.

Table 1. Activation Products in Potential Nuclear Waste Materials

Matrix Material	Activated Species	Activity[a]
Copper	^{182}Ta	1.3 E+6
	^{124}Sb	2.0 E+5
	^{110}Ag	2.7 E+5
	^{65}Zn	1.6 E+5
	^{75}Se	1.1 E+5
Aluminum	^{182}Ta	5.7 E+5
	^{59}Fe	4.4 E+5
	^{65}Zn	2.3 E+5
	^{51}Cr	5.2 E+5
Lead	^{124}Sb	4.1 E+8
	^{110}Ag	3.5 E+6
Zircaloy	^{95}Zr	2.3 E+8

(contd)

Table 1. (contd)

Matrix Material	Activated Species	Activity[a]
Titanium	^{51}Cr	3.8 E+6
	^{59}Fe	4.1 E+5
	^{124}Sb	1.3 E+5
	^{182}Ta	2.0 E+5
Zinc glass	^{65}Zn	1.0 E+8
	^{124}Sb	3.5 E+6
Soft glass	^{65}Zn	2.3 E+6
	^{124}Sb	1.0 E+6
	^{110}Ag	1.1 E+5
	^{134}Cs	8.1 E+5
Porcelain beads	^{46}Sc	1.2 E+7
	^{51}Cr	4.0 E+6
	^{134}Cs	1.0 E+5
	^{152}Eu	4.0 E+5
Borosilicate glass	^{60}Co	1.7 E+3
	^{65}Zn	2.8 E+3
	^{110}Ag	1.2 E+4
	^{124}Sb	7.2 E+7
	^{134}Cs	2.7 E+3
	^{152}Eu	2.7 E+3

[a]Activity in units of disintegrations per minute (*i.e.*, time at end of irradiation) per gram of irradiated matrix material.

Results of three sequential leach tests for a variety of materials, using quiescent 25°C distilled water as leachant, are given in Table 2. (The leach rates for the 48-d leach test were presented in [STEINDLER-1979B].) The results of the leach rate measurements for titanium (identified in Table 1) were questionable because of the low leach rate for this material, coupled with the low activities for the activated species. Hence, results for titanium were not reported in Table 2. The weight loss data in Table 2 are based on small differences between large numbers and hence are subject to considerable uncertainty.

The aluminum samples studied actually gained weight in the sequential leach tests, indicating probable oxide formation. The aluminum-12% silicon alloy had a significantly higher rate of removal (*i.e.*, about 40-fold) than did commercial grade aluminum metal (Table 2). (Silicon is added to aluminum used as a metal matrix to improve its casting characteristics.) These results indicate that the addition of silicon may reduce the resistance of the aluminum to aqueous corrosion. It must be remembered that because of their amphoteric behavior, metals such as lead and aluminum are particularly sensitive to pH variations. Hence, it is important that studies of these metals be done with the particular aqueous media that will be encountered in geologic storage.

Table 2. Sequential Incremental 25°C Leach[a] Rates in Quiescent Water for Various Materials Associated with Nuclear High-Level-Waste Studies

Matrix Material	Activated Species Measured	Leach Rate, $g/cm^2 \cdot d$[b] 1st (48d)[c]	2nd (50d)[c]	3rd (90d)[c]
Copper	^{182}Ta	2.7 E-6	6.0 E-6	1.8 E-6
	^{75}Se	3.0 E-6	5.1 E-6	--
	^{65}Zn	--	5.5 E-6	--
	wt loss[d]			6.3 E-7
Aluminum	^{65}Zn	--	1.6 E-6	0.9 E-6
	^{182}Ta	1.5 E-6	--	--
	wt loss[e]			--
Aluminum-12% Silicon	^{65}Zn	6.6 E-5	--	--
Zircaloy	^{95}Zr	2.1 E-9	3.0 E-9	--
Lead	^{110}Ag	4.8 E-6	7.3 E-6	8.5 E-7
	^{124}Sb	2.0 E-5	6.0 E-5	1.7 E-5
	wt loss[d]			1.5 E-4
Porcelain	^{46}Sc	1.2 E-8	1.3 E-8	5.0 E-9
	^{134}Cs	5.5 E-6	4.3 E-6	--
	wt loss[d]			8.8 E-8
Soft glass	^{65}Zn	2.5 E-7	2.1 E-7	3.0 E-8
	^{110}Ag	--	2.0 E-7	2.3 E-7
	^{124}Sb	9.7 E-7	1.1 E-6	1.7 E-7
	^{134}Cs	1.7 E-7	5.2 E-7	8.4 E-8
	wt loss[d]			7.7 E-7
Zinc glass	^{65}Zn	7.0 E-8	6.7 E-8	4.4 E-8
	wt loss[d]			2.3 E-7
Borosilicate glass	^{124}Sb	3.2 E-7	5.8 E-8	1.4 E-8
	^{134}Cs	3.1 E-5	4.6 E-6	1.3 E-6
	wt loss[d]			9.3 E-8

[a] Leaching medium was quiescent distilled water (pH 5.8).

[b] These units of grams per cm^2 per day ($g/cm^2 \cdot d$) represent the equivalent grams that would have been leached if the entire matrix leached at the same rate as the isotope studied.

[c] Duration of each sequential leach test in days.

[d] Weight loss data are based on small differences between large numbers and hence is subject to considerable uncertainty.

[e] Aluminum samples showed weight gains, indicating probable oxide formation.

Within the uncertainties of these determinations, the metals studied showed no change in leach rate with time. This behavior is consistent with what would be expected for material that was being removed by surface erosion. For these purposes, it is more meaningful to report the leach rates ($g/cm^2 \cdot d$) in units of a penetration rate (cm/d). Details of this conversion and its significance have been reported previously [STEINDLER-1979B].

For all matrix materials studied, the leach rates (*i.e.*, the rates of removal) were based on the assays of trace elements present in the matrix except for Zircaloy, in which case ^{95}Zr was measured. These measurements can always be questioned on the basis that the trace elements may not leach as does the matrix material. Calibration of the behavior of the radioactive trace element with matrix material removal by weight loss measurement is difficult for a variety of reasons. For example, weight losses at low leach rates are based on measurements of small differences between large numbers. Also, many metals (*e.g.*, aluminum) form oxide coatings on the surface, preventing measurement of weight losses.

Because of these uncertainties, it would be desirable to base determinations of metal penetration rates on radioactive species that are closely allied with the matrix material. Activated species produced by neutron reactions on the metals being considered are identified in Table 3. As can be seen from this table, studies of aluminum must still depend on measurement of trace metal concentration. Iron, stainless steel, Zircaloy, and brass are adequately monitored by (n, γ) reactions on the host material. Copper, lead, and titanium can be more precisely studied by way of (n, p) and (n, α) reaction products. For these purposes, higher energy neutrons than those available from research reactors would be desirable, and a 14-Mev neutron generator located at ANL is available. Experiments are in progress to determine the usefulness of this machine for these studies.

Some preliminary data are presented in Table 4 for leach rates of metals, based on weight loss when saturated WIPP brine was used as the leachant. Determinations were made at both 25°C and 109°C. Leach rates for 25°C water were taken from Table 2 and are included for comparison purposes. These results indicate significantly accelerated rates of destruction in saturated WIPP brine, particularly at the higher temperature. Further investigation using the neutron activation technique seems warranted and will be pursued. Measurement of aluminum leach rate was not possible because of weight gains--presumably due to surface oxide formation.

Leach rates of samples of porcelain and various types of glass are also included in Table 2. These materials represent simulated waste matrix substances. Of interest is the rate at which specific hazardous radionuclides (*e.g.*, ^{137}Cs) will be leached from the matrix. Cesium, as well as several other elements, were investigated. The leach rates decreased as a function of time, indicating at least some contribution from diffusion in the solid matrix. Also, there were significant variations in leach rate for different elements from the same matrix. This behavior is symptomatic of diffusion phenomena. In general, it was observed that the leach rates, specific activities of the leached ions, and leaching behavior (*i.e.*, leach rate *vs.* time) are about the same for all of these materials.

Table 3. Activated Species from High-Energy (Fast) Neutron Activation of Metals

Metal	Reaction	Product Species	Product Characterization $T^{1/2}$	Radiation
Aluminum (Al)	(n, α)	^{24}Na[a]	15h	β, γ
Copper (Cu)	(n, α)	^{60}Co	5.3y	β, γ
Iron (Fe)	(n, p)	^{54}Mn	312d	γ
	(n, γ)	^{59}Fe	45d	β, γ
Lead (Pb)	(n, p)	^{204}Tl	318y	β
	(n, α)	^{203}Hg	47d	β, γ
Stainless steel (Co)	(n, γ)	^{60}Co	5.3y	β, γ
Titanium (Ti)	(n, p)	^{46}Sc	84d	β, γ
Zircaloy (Zr)	(n, γ)	^{95}Zr	64d	β, γ
Brass (Zn)	(n, γ)	^{65}Zn	244d	β, γ

[a]Because of the short half life of ^{24}Na, it is useful for short-term studies only (*i.e.*, 5 days or less).

Table 4. Leach Rates (Weight loss method) for Metals Using Saturated WIPP Brine as Leachant

Material	Surface Area, cm^2	Weight, g	Leach Rate, $g/cm^2 \cdot d$		
			WIPP Brine		Water[a]
			25°C	109°C	25°C
Stainless Steel	21.1	7.3	1.5 E-6	6.9 E-5	--
Copper	17.0	5.5	6.5 E-5	6.1 E-4	6.3 E-7
Lead	11.3	15.0	1.0 E-4	1.6 E-3	1.5 E-4
Zircaloy(^{95}Zr)[b]	4.2	1.2	5.1 E-9	6.9 E-8	2.1 E-9

[a]Data from Table 2 of this report.

[b]Leach rates based on weight loss could not be determined for this material because they were low. However, leach rates based on ^{95}Zr levels before and after leaching were obtained.

Studies of the leach resistance of proposed solid high-level waste forms have centered around borosilicate glasses, with particular emphasis on a formulation prepared by Battelle Pacific Northwest Laboratories (PNL) and identified as 76-68 waste glass [McELROY-1977].

Two forms of this waste glass were obtained from PNL. These consisted of uranium-spiked glass (discs of about 2.3 cm^2 surface area, each weighing 0.3 g) and glass spiked with plutonium-neptunium (beads of 1.5 cm^2 surface area, each weighing 0.35 g). The surface areas given above are based on calculations from geometric shapes. Leach rates were determined for as many as twenty different chemical elements, using four different leaching media at three different temperatures [ambient room temperature (∿25°C), boiling aqueous (∿100°C), and high-pressure autoclave (∿280°C)]. Some of these data were reported previously [STEINDLER-1979B].

Of the variables associated with leaching, temperature has the most significant effect on the leach rate. Results of initial seven-day leach tests (using distilled water leachant) for a dozen prominent elements are summarized in Table 5. The leach rate data for ^{137}Cs and ^{152}Eu are plotted as a function of temperature in Fig. 1. The leach rate for cesium increased by four orders of magnitude as the temperature increased from 25°C to ∿280°C. The effect of temperature on the leach rate for europium was much less (*i.e.*, a change of about one order of magnitude over the same temperature range). These two elements (cesium and europium) represent the extremes for this temperature effect among the hazardous waste elements studied in these experiments. Because of their chemical similarity, the trivalent actinides ought to behave in a manner analogous to europium. The results for uranium and neptunium (Table 5) indicate that the effect of temperature on leaching of these elements would be only marginally greater than that observed for europium.

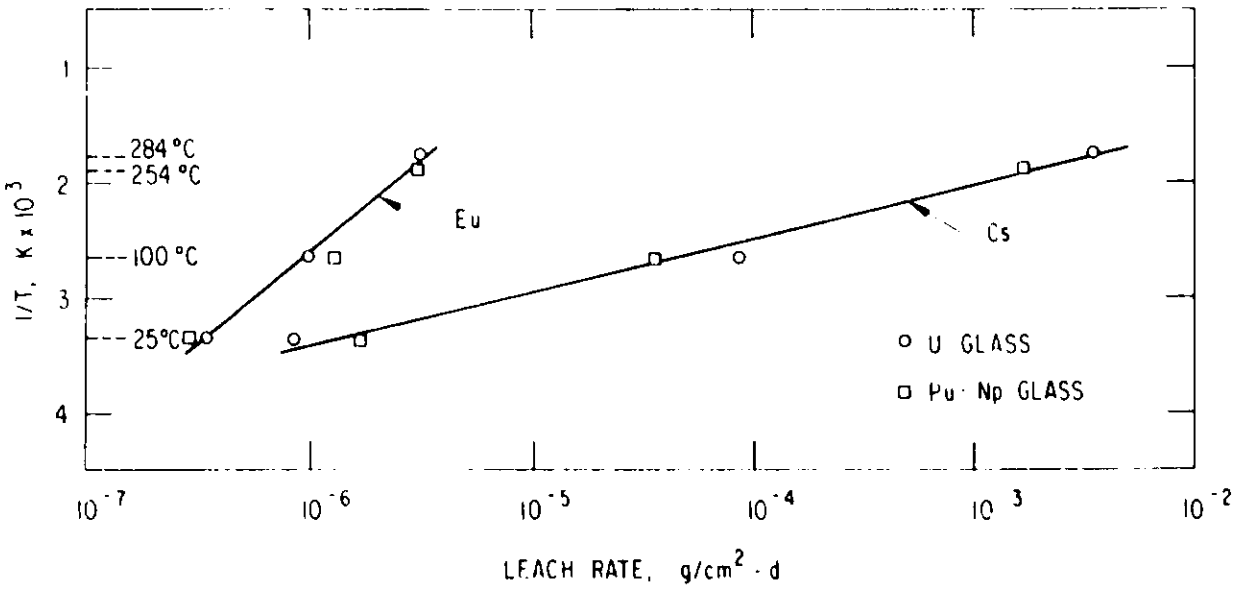

Fig. 1. Effect of Temperature on Leach Rate

Table 5. Leach Rates for PNL 76-68 Glass at Indicated Temperatures

Isotope Determined	Incremental Leach Rate,[a] g/cm^2·d					
	U-Spiked Glass			Pu-Np Spiked Glass		
	25°C	100°C	286°C	25°C	100°C	254°C
^{60}Co	4.8 E-6	3.4 E-5	6.6 E-5	1.5 E-6	1.1 E-5	6.8 E-5
^{65}Zn	4.9 E-6	1.6 E-5	4.5 E-5	1.6 E-6	1.6 E-5	b
^{95}Zr	4.5 E-7	2.4 E-6	1.1 E-5	1.5 E-7	2.8 E-6	1.0 E-4
^{103}Ru	1.2 E-6	7.4 E-6	b	1.7 E-6	4.8 E-6	b
^{110m}Ag	1.9 E-6	2.9 E-5	b	1.3 E-6	3.2 E-5	b
^{131}I	1.5 E-6	b	1.1 E-3	7.1 E-6	3.9 E-5	2.6 E-3
^{134}Cs	8.4 E-7	8.9 E-5	3.5 E-3	1.7 E-6	3.6 E-5	1.7 E-3
^{140}Ba	1.8 E-6	1.5 E-5	b	5.5 E-7	5.9 E-6	b
^{141}Ce	6.5 E-7	1.2 E-6	2.6 E-6	2.5 E-7	2.3 E-6	b
^{152}Eu	3.5 E-7	1.0 E-6	3.3 E-6	2.9 E-7	1.3 E-6	3.2 E-6
^{237}U	5.9 E-7	b	b	7.2 E-7	3.1 E-6	b
^{239}Np	b	b	b	7.1 E-6	2.4 E-5	2.7 E-4

[a] Each leach test was for seven days in distilled water.

[b] These data were not resolvable from the gamma spectra.

Sequential tests are in progress to measure leaching as a function of time under the conditions given in Table 5. Accumulated results of these tests are tabulated in Tables 6 through 8. Leach rates for six or seven isotopes are reported in these tables. Leach rates for many other elements have been determined, but these six are deemed the most representative and the least ambiguous in terms of analyses of the counting data. The leach rates are observed to decrease slowly with time, a phenomenon commonly observed in leach studies and attributed to the effects of diffusion in the solid phase.

The data for cesium in Table 8 have been plotted in Fig. 2. At all three temperatures, the observed decrease in leach rate is approximately linear (*i.e.*, slope is approximately -1) with time for the time interval studied (about 60 days). Similar results have been reported previously [STEINDLER-1979A], using other waste forms. Diffusion theory predicts a time to the ~1/2 time dependence. This phenomenon is being studied in greater detail in order to establish the consequences of this process on long-term waste disposal.

Plutonium was not analyzed for in this series of experiments. However, samples are available for dissolutions and radiochemical separations whereby plutonium and neptunium may be determined by low-level alpha counting techniques.

Table 6. Sequential Leach Rates for (76-68) PNL-Glass[a] (Uranium-Spiked) in 25°C Distilled Water

	Incremental Leach Rate, $g/cm^2 \cdot d$[b]									
	1st	2nd	3rd	4th	5th	6th	7th	8th	9th	10th
	5.8[c]	21.0[c]	32.0[c]	29.1[c]	48.9[c]	49.0[c]	54.1[c]	50.0[c]	51.0[c]	52.7[c]
	5.8[d]	26.8[d]	58.8[d]	87.9[d]	136.8[d]	185.8[d]	239.9[d]	289.9[d]	340.9[d]	393.6[d]
Isotope	2.9[e]	16.3[e]	42.8[e]	73.4[e]	112.4[e]	161.3[e]	212.9[e]	264.9[e]	315.4[e]	367.3[e]
^{60}Co	4.8 E-6	1.4 E-6	1.2 E-6	4.1 E-6	1.8 E-7	1.2 E-7	5.2 E-7	f	4.3 E-7	4.7 E-7
^{65}Zn	5.4 E-6	8.7 E-7	6.5 E-7	1.8 E-7	1.5 E-8	1.5 E-8	3.5 E-7	6.6 E-7	3.3 E-7	5.0 E-7
^{85}Sr	5.8 E-6	1.1 E-6	9.6 E-7	1.5 E-6	6.6 E-7	1.3 E-6	2.1 E-6	f	f	f
^{110}Ag	1.9 E-6	f	2.8 E-7	7.3 E-7	1.7 E-7	f	5.0 E-7	f	3.2 E-7	6.9 E-7
^{134}Cs	7.8 E-7	2.9 E-7	6.1 E-7	4.4 E-7	5.2 E-8	1.3 E-7	4.2 E-7	2.2 E-7	1.6 E-7	1.7 E-6
^{141}Ce	6.0 E-7	7.1 E-8	1.2 E-7	1.2 E-7	f	f	f	f	f	f
^{152}Eu	5.1 E-7	6.5 E-8	8.4 E-8	3.1 E-8	3.2 E-9	2.7 E-9	3.7 E-7	3.5 E-7	8.8 E-8	4.6 E-7
Wt Loss[g]										1.8 E-6

[a] Glass composition defined in [McELROY-1977].

[b] These units of grams per cm^2-day ($g/cm^2 \cdot d$) represent the equivalent grams that would have been leached if the entire matrix had leached at the same rate as the specific isotope studied.

[c] Length of time (in days) for each sequential leach test.

[d] Cumulative time of leaching for each test.

[e] Median leach time for each test.

[f] These data have not been resolved from the gamma spectrum.

[g] The weight loss data are based on the integrated weight loss over all of the sequential leach tests to date.

Table 7. Sequential Leach Rates for (76-68) PNL-Glass[a] (Uranium-Spiked) in Distilled Water

	Incremental Leach Rate, $g/cm^2 \cdot d$[b]						
	100°C					254°C	
	1st	2nd	3rd	4th	5th	1st	2nd
	8.8[c]	25.0[c]	24.1[c]	39.0[c]	64.8[c]	16.0[c]	40.0[c]
	8.8[d]	33.8[d]	57.9[d]	96.9[d]	161.7[d]	16.0[d]	56.0[d]
Isotope	4.4[e]	21.3[e]	45.9[e]	77.4[e]	129.6[e]	8.0[e]	36.0[e]
^{60}Co	4.4 E-5	1.5 E-5	3.7 E-6	1.5 E-6	7.9 E-6	6.6 E-5	2.3 E-5
^{65}Zn	1.6 E-5	8.3 E-6	3.7 E-6	2.0 E-6	1.7 E-6	7.2 E-6	7.7 E-7
^{110}Ag	2.4 E-4	2.9 E-5	9.6 E-6	4.4 E-6	4.3 E-6	f	7.7 E-6
^{134}Cs	6.6 E-5	2.1 E-5	9.1 E-6	7.5 E-6	1.5 E-6	4.7 E-4	1.4 E-4
^{141}Ce	1.0 E-6	1.7 E-7	3.2 E-6	8.5 E-7	f	2.6 E-6	4.9 E-7
^{152}Eu	1.0 E-6	2.3 E-7	2.3 E-6	4.2 E-7	7.0 E-7	2.2 E-6	4.9 E-7
Wt Loss[g]					3.0 E-6		3.4 E-4

[a] Glass composition defined in [McELROY-1977].

[b] These units of grams per day cm^2-day ($g/cm^2 \cdot d$) represent the equivalent grams that would have been leached if the entire matrix had leached at the same rate as the specific isotope studied.

[c] Length of time (in days) for each sequential leach test.

[d] Cumulative time of leaching for each test.

[e] Median leach time for each test.

[f] These data have not been resolved from the gamma spectrum.

[g] The weight loss data are based on the integrated weight loss over all of the sequential leach tests to date.

Table 8. Sequential Leach Rates for 76-68 PNL Glass[a] (Plutonium-Spiked) in Distilled Water

Isotope	Incremental Leach Rate, $g/cm^2 \cdot d$[b]								
	25°C			100°C			254°C		
	1st	2nd	3rd	1st	2nd	3rd	1st	2nd	3rd
	6.9[c]	13.0[c]	42.0[c]	7.0[c]	13.2[c]	41.8[c]	7.0[c]	11.9[c]	40.8[c]
	6.9[d]	19.9[d]	61.9[d]	7.0[d]	20.2[d]	62.0[d]	7.0[d]	18.9[d]	59.7[d]
	3.5[e]	13.4[e]	40.9[e]	3.5[e]	13.6[e]	41.1[e]	3.5[e]	13.0[e]	39.3[e]
^{60}Co	1.5 E-6	f	1.3 E-6	1.1 E-5	4.1 E-5	f	5.3 E-5	4.7 E-5	1.5 E-5
^{65}Zn	1.6 E-6	f	2.3 E-7	1.6 E-5	8.2 E-6	4.2 E-7	f	1.3 E-5	1.9 E-6
^{110}Ag	1.3 E-6	f	3.2 E-7	3.2 E-5	5.1 E-6	3.6 E-6	f	f	f
^{134}Cs	1.7 E-6	1.2 E-6	2.2 E-7	3.6 E-5	3.5 E-5	4.2 E-6	1.7 E-3	1.1 E-3	3.7 E-4
^{141}Ce	2.5 E-7	f	5.1 E-7	2.3 E-6	4.9 E-7	2.0 E-7	f	f	f
^{152}Eu	2.9 E-7	3.0 E-7	2.4 E-7	1.3 E-6	5.4 E-7	1.1 E-7	3.2 E-6	1.5 E-6	8.5 E-7
Wt Loss[g]	(not determined)					3.2 E-6			4.8 E-4

[a] Glass composition defined in [McELROY-1977].

[b] These units of grams per cm^2-day ($g/cm^2 \cdot d$) represent the equivalent grams that would have been leached if the entire matrix had leached at the same rate as the specific isotope studied.

[c] Length of time (in days) for each sequential leach test.

[d] Cumulative time of leaching for each test.

[e] Median leach time for each test.

[f] These data have not been resolved from the gamma spectrum.

[g] The weight loss data are based on the integrated weight loss over all of the sequential leach tests to date.

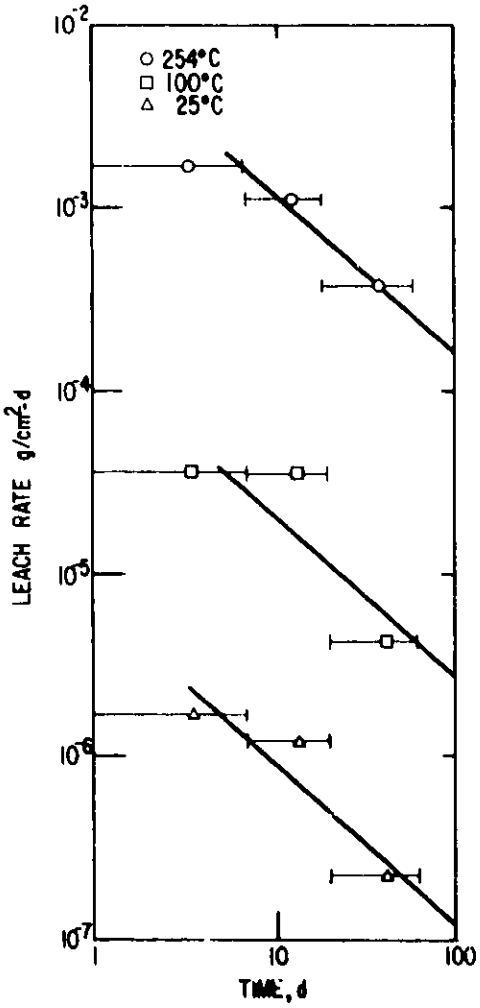

Fig. 2. Leach Rates for Cesium from PNL-Glass

A low-background beta counting system has been purchased from the Tennelec Corporation and installed. This system counts automatically and corrects for dead-time losses. Preliminary testing indicates that this instrument will allow us to determine leach rates for non-γ-emitting nuclides (*e.g.*, ^{99}Tc and ^{90}Sr) and to greatly increase sensitivity for all nuclides. This system is also capable of counting alpha emitters. There is also a capability for incorporating a gamma-ray detector into the system. This capability allows simultaneous gamma ray analysis and/or beta-gamma coincidence counting. A counter background of 0.58 ± 0.02 c/m beta and 0.032 ± 0.007 c/m alpha has been established. Additional testing is in progress to establish the counter efficiency.

3. Conclusions

The neutron activation analysis technique has been shown to be potentially applicable for measuring the rate of removal or penetration of many metals being considered as geologic disposal containers or barriers. Time-sequential leach tests show no change in leach rate with time, indicating that these metals are being removed by surface erosion. Studies of alloys (*e.g.*, aluminum-12% silicon) show that as might be expected, penetration rates can be very sensitive to alloying materials.

Of the variables associated with the leaching medium, temperature was shown to have the most significant effect on the leach rates of borosilicate glasses. Results indicate that the leach rate for cesium from PNL 76-68 glass is particularly sensitive to temperature, increasing by four orders of magnitude as the temperature is increased from 20°C to 280°C. The effect of the same temperature range on the leach rate for europium (a trivalent rare earth) was much less (*i.e.*, about one order of magnitude over the same temperature range).

B. Characterization of Impact Fracture of Brittle Solid-Waste Forms (W. J. Mecham, L. J. Jardine, and R. Pelto)

1. Introduction

The fracture of solid-waste forms that could occur as a result of mechanical impacts during in-plant handling and storage and during off-site transportation needs to be known to evaluate the risk of dispersion of radioactive wastes. Two physical properties of the waste form which may be useful to characterize increased dispersion risks from fracture are the increase in surface area and the (mass) fraction of particles smaller than the respirable size (*i.e.*, <10 μm). An analysis and evaluation of the effects of impacts have been initiated for metal-encapsulated reference glass and ceramic waste forms. Descriptive and calculational models were developed for relating impact energy to deformation effects (for both brittle and ductile materials) to characterize the surface area resulting from impact fracture of brittle materials [MECHAM-1980B].

Here, a methodology is presented for analyzing particle size distributions obtained in impact-testing of brittle waste-form materials. The methodology includes (a) a linear two-parameter lognormal correlation of the weight fraction smaller than any given size, (b) a mathematical function of the two lognormal parameters to determine the total surface area in terms of a dimensionless shape factor, and (c) a surface-energy constant to predict the increase in surface area from the known energy absorbed in the impact of the brittle material. Preliminary measurements were made on impacted simulated glass specimens. The analysis is used as an example of the methodology. These results are also compared with reanalyzed impact test data reported by others.

2. Deformation of Brittle Materials by Mechanical Impact

Brittle fracture of typical glass or ceramic solids under an impact results in fragmentation and the formation of new surface area (ΔS_F). Fracture energy (W_F) absorbed in the brittle material is proportional to ΔS_F over a considerable range of energy inputs for a given specimen and mode of impact. The proportionality constant is termed the fracture surface energy, γ_F [MECHAM-1980B]. Thus,

$$W_F = \gamma_F \Delta S_F \qquad (1)$$

In Eq. 1, W_F is generally smaller than the gross impact-energy input (W_I), due to deformation in the test equipment. Even for "bare" glass specimens impacted by hard steel surfaces, deformation of the ductile metal typically absorbs more than 50% of the gross impact energy (W_I). Variation of γ_F can be expected for different specimen materials, sizes, and shapes and for variations of input energy concentrations in specimen volumes (V_o).

In the work on brittle fracture of Piret and associates [AXELSON, KENNY, ZELENY] both single impacts and slow-compression crushing were applied to (1) small ($\sim$1.5 cm^3) solid specimens (spheres and cylinders) of Pyrex glass and (2) prisms of natural quartz at input energy densities up to 17 J/cm^3. Multiple impacts and slow-compression crushing were applied to particulate samples (10-14 mesh) of natural quartz. The principal result was a measurement of the net energy absorbed (W_F) in the brittle materials in producing the new surface area measured by a gas adsorption technique. Calorimetric methods were used to establish the net energy absorbed. Results were presented as plots of the net energy density (W_F/V_o) applied in impacting specimens *vs.* the net fracture-surface energy, γ_F. By way of introduction, a representative selection of the data points (Fig. 3) is repeated from the preceding quarterly report [STEINDLER-1979B]. There is a great deal of scatter in the slow-compression data for a given test material, *e.g.*, 10-fold variations of γ_F (4 to 80 J/m^2) for the given range of values of W_F/V_o. However, for impact fracture, γ_F was nearly constant ($\sim$100 J/m^2) while W_F/V_o varied by more than two orders of magnitude. This implies that Eq. 1 may be used to estimate ΔS_F for an impact input energy W_F, since γ_F is reasonably constant for many energy densities.

3. The Lognormal Particle-Size Distribution

It is shown below that the particulate solids formed in brittle fracture exhibit a particle-size distribution that can be described by the lognormal probability function. (Details as to why this is the fundamental relationship to be expected based on the physical laws will be given in a separate paper [MECHAM-1980A]. This function has two parameters obtainable from graphical analysis--namely, the geometric mean diameter, D_g, and the geometric standard deviation, σ. D_g is the diameter at the 50% mass fraction, and σ is the ratio of the diameters plotted at 50% and 16% mass fractions. The ratio (S_F/V_o) of total particulate surface area to solid volume, can be expressed [HERDAN] as a particulate "equation of state" in terms of the lognormal parameters as

$$\frac{S_F}{V_o} = \frac{\alpha\sigma^{0.5} \ln \sigma}{D_g} \tag{2}$$

where α is a dimensionless shape factor. The minimum value of α is 6 (for spheres and cubes). For brittle fragments of other shapes, α is typically 2 to 3 times greater. The total particulate surface area, S_F, is related to the original specimen surface area, S_o, and to the surface area formed in fracture, ΔS_F by

$$\Delta S_F = S_F - S_o \tag{3}$$

The relations expressed by the three above equations provide quantitative parameters which can serve as a basis for systematic test programs for characterizing the results of impact on various composite bodies of brittle and ductile materials, such as canistered glass waste forms or metal-encapsulated composites.

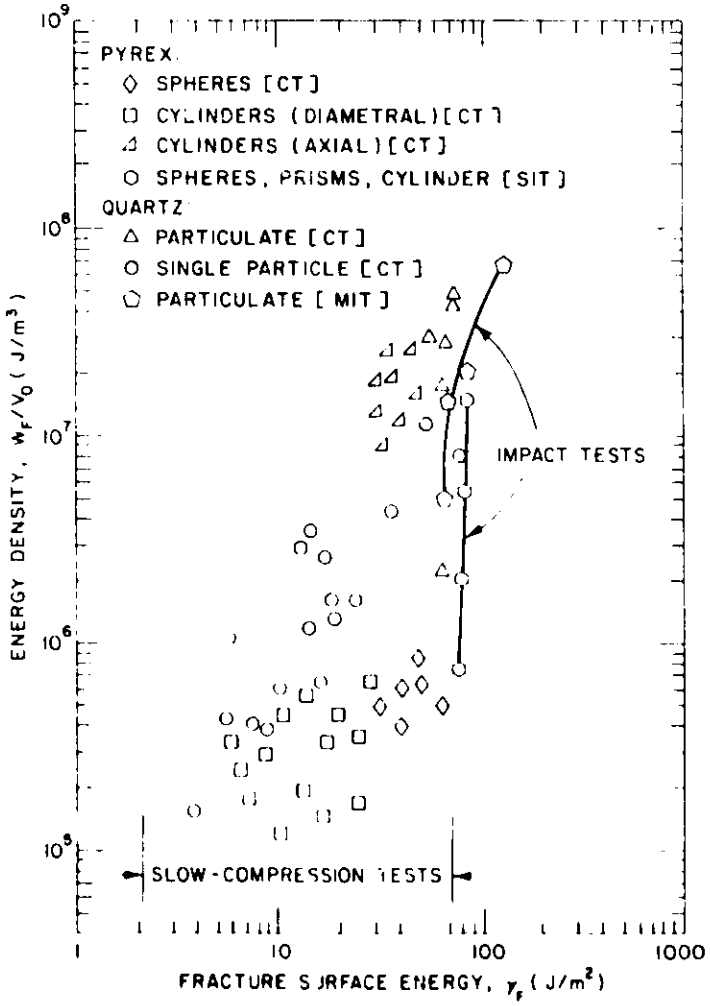

Fig. 3. Results of Measurements [AXELSON, KENNY, ZELENY] of the Fracture Surface Energy, γ_F, of Pyrex and Quartz at Various Specimen Net Impact Energy Densities for Compression Tests [CT], Single Impact Tests [SIT] and Multiple Impact Tests [MIT]. ANL Neg. No. 308-79-789

4. Application of the Energy and Size Relationships to Impact Testing

Two 5.3-g samples, each consisting of 19 Pyrex spheres (6.2-mm), were impacted by a drop-weight device at two energy densities, 6.9×10^6 and 3.3×10^6 J/m^3, based on gross impact energy input. The net energy input was not measured. Size distributions were measured by sieve analyses and are labeled ANL-1 and ANL-2 in Table 9. The fracture surface area was also measured for one test (ANL-2) by (Kr) gas BET adsorption. The cumulative lognormal plots of these particle sizes are given in Fig. 4. The linearity of the plots is important for estimating the cumulative mass fraction of respirable sizes (<10 μm). The lognormal parameters from the graphical analysis and the calculated fracture-surface energies are also shown in Table 9. The fracture-surface area for test ANL-1 was calculated from the lognormal surface/volume ratio (S_P/V_O in Table 9) with the value of the shape factor $\alpha = 12$ as determined from test ANL-1.

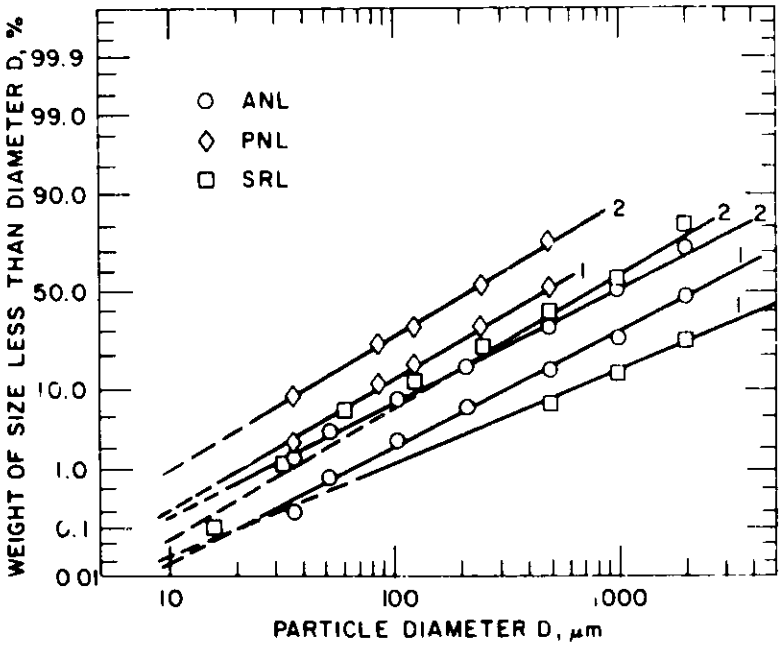

Fig. 4. Cumulative Lognormal Plot of Measured Particle Size Distributions for Various Impact Tests of Glass Materials. ANL Neg. No. 308-79-792

To allow comparison, data selected from the literature on the impact fracture of brittle materials representative of solid waste forms are also reported in Table 9 and Fig. 4. Tests on two materials impacted at two different energy densities at the Savannah River Laboratory (SRL) [WALLACE] were: (1) a simulated borosilicate waste glass in the form of a cylindrical specimen, 0.50 in. dia and 1.0 in. long, and (2) a concrete in the form of a "neat" high-alumina cement cylinder, 1.0-in. dia and 0.50-in. long.

Table 9. Selected Test Data on Impact Fracture of Brittle Specimens

	ANL-1	ANL-2	SRL-1	SRL-2	PNL-1	PNL-2
MATERIAL	Pyrex Beads	Pyrex Beads	B-Glass Cyl	B-Glass Cyl	SL Glass Cyl	SL Glass Cyl
VOLUME, V_o, cm^3	2.38	2.38	3.33	3.33	1.25	1.25
SURFACE, S_o, cm^2	23	23	12.7	12.7	12.8	12.8
SURFACE, S_F, cm^2	424 (calc'd)	1000 (meas'd)	354 (calc'd)	1320 calc'd)	1540 (meas'd)	2870 (meas'd)
ENERGY, $\frac{W_i}{V_o}$, $\frac{J}{m^3}$	3.3×10^6	6.9×10^6	5.9×10^6	2.4×10^7	2.2×10^7	8.9×10^7
Lognormal parameters:						
D_g, μm	2100	930	7000	750	470	225
σ	4.7	4.6	6.7	3.8	3.8	3.8
Wt % D ≤10 μm	0.02	0.32	0.03	0.06	0.20	0.90
$\frac{S_F}{V_o}$, $\frac{1}{m}$	1.46×10^3	3.44×10^3	8.72×10^2	3.25×10^3	5.19×10^3	1.08×10^4
γ_F J/m^2	1.8×10^2	1.6×10^2	5.6×10^2	6.0×10^2	1.8×10^2	3.9×10^2

Two tests made at Battelle Pacific Northwest Laboratory (McELROY-1977] used a reference commercial soda-lime silica glass in the form of cylinders, 0.44-in. dia and 0.50 in. long.

Engineering studies of impact effects on fuel capsules (for aerospace applications) were made at Monsanto Mound Laboratory [BONNELL]; two impact tests of PuO_2 microspheres sealed into a stainless steel (6 1/2-in. long x 7/8-in. OD with 3/8-in. walls) capsule were reanalyzed. Only data from the glass specimens are reported in Table 9. However, all particle size data, when replotted lognormally as in Fig. 4, formed straight lines, and all values of σ (from graphical analysis) were in the range shown for the glass specimens.

Analysis of the above data shows that for a given material, σ is nearly constant over a range of energy densities. The D_g varies inversely with the energy density. The particulate surface area, as determined directly by gas adsorption or as calculated from the lognormal parameters and the shape factor $\alpha = 12$, allows fracture-surface energy, γ_F (J/m^2), to be calculated if the net energy is known. For impacts, γ_F appears to be nearly constant for a given material, and to increase at higher energy densities (W_F/V_O). The energies reported here are the total input energies; the net energy absorbed in brittle fracture is expected to be lower by a factor of about two for "bare" specimens and by a factor of more than four for canistered specimens. The considerable uniformity in lognormal relationships of these tests of different specimens under quite varied test conditions are promising as a basis of further systematic tests and analyses.

Three small cylindrical specimens of different glass compositions were impacted [McELROY-1977] at four different energies. Particle sizes were measured by sieving, and the original results were presented in linear plots (not presented here). Fracture surface areas were not reported. To test the methodology on different glass compositions, the particle size data were replotted on lognormal graphs to determine the two lognormal parameters and the surface areas. These lognormal plots are shown in Fig. 5, and the lognormal parameters, calculated surface areas and fracture-surface energies are shown in Table 10. From reported data [McELROY-1977] on surface areas of typical particle size distributions of soda-lime-silica glass, a mean shape factor of $\alpha = 21 \pm 3$ was calculated. This value was used to calculate surface areas from the lognormal S_F/V_O ratio given in Eq. 2. These parameters show the comparative fracture properties of the materials. The constancy of the values of σ is striking, as shown by the similar slopes in Fig. 5.

To obtain a range of impact energies, multiple impacts on a single specimen have been used at SRL and PNL. For example, tests of the same type of specimen were made with the same total energy-input density, but with that total energy applied in either 1, 2, 4, and 8 blows (McELROY-1977]. The size distributions have been plotted lognormally in Fig. 6. From the lognormal parameters, the highest energy density (1 blow) showed the smallest D_g, the largest γ_F, and the smallest S_F/V_O. The principal difference was the quantity of respirable fraction (<10-μm dia), which was 1.3% for 1 blow and 6.6% for 8 blows. This effect is consistent with other brittle-fracture data [STEINDLER-1979B]

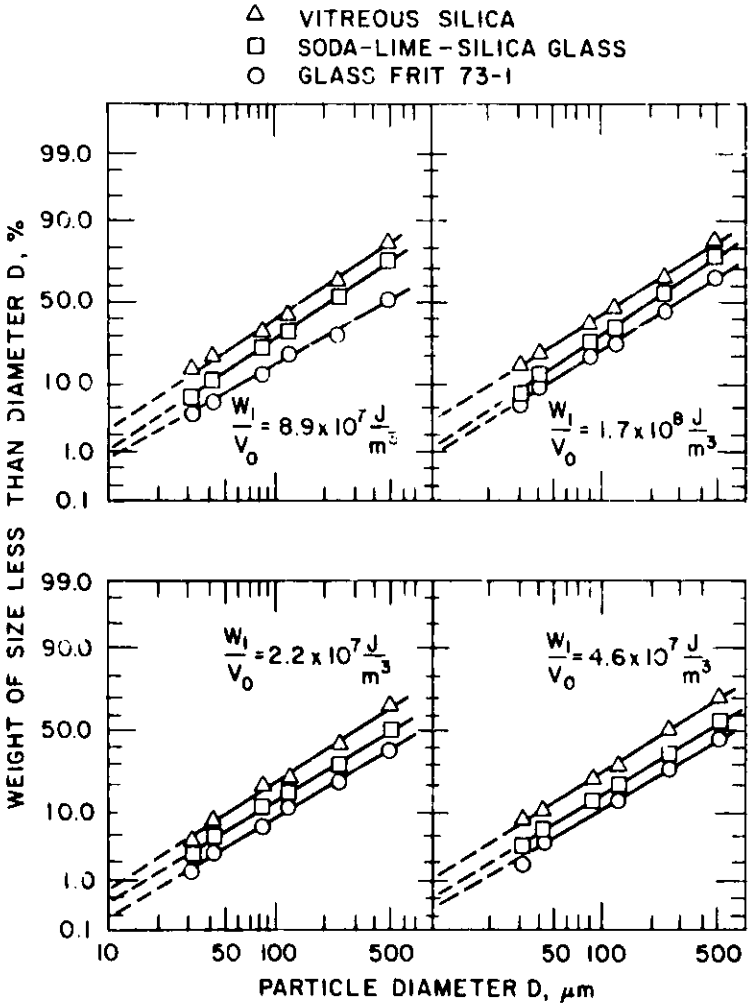

Fig. 5. Lognormal Plots of Data Reported [McELROY-1977] for Three Types of Impacted Glass Compositions at Four Energy Densities. ANL Neg. No. 308-79-790

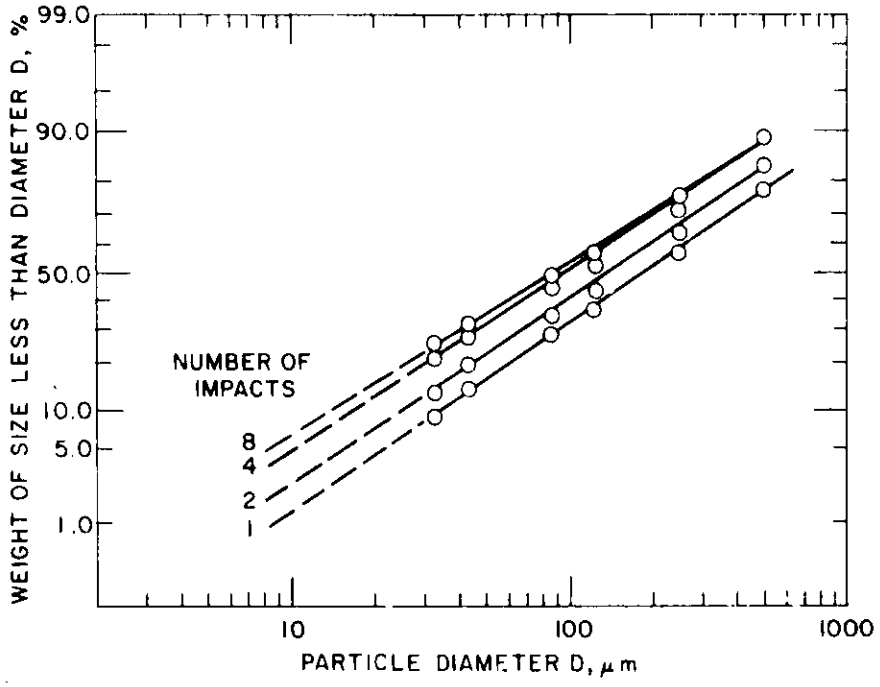

Fig. 6. Lognormal Plot of Data Reported [McELROY-1977] for Impacted Glass Specimens Receiving the Same Total Energy but with a Different Number of Impacts. ANL Neg. No. 308-79-791

Table 10. Lognormal Parameters of Impact Fracture of Three Different Glass Compositions

Glass Type	W/V, J/m^3	D_g, μm	σ	Wt % (D<10 μm)	S/V, m^{-1}	Calc γ_F, J/m^2
Soda-lime-silica Glass	1.70×10^8	192	3.7	1.2	3.75×10^5	4.5×10^2
	8.9×10^7	220	3.7	0.8	2.47×10^5	3.6×10^2
	4.6×10^7	370	4.1	0.6	1.65×10^5	2.8×10^2
	2.2×10^7	490	4.4	0.4	1.19×10^5	1.8×10^2
Frit	1.7×10^8	290	4.3	1.0	2.1×10^5	8.1×10^2
	8.9×10^7	490	4.4	0.4	1.3×10^5	6.8×10^2
	4.6×10^7	530	4.4	0.4	1.2×10^5	3.8×10^2
	2.2×10^7	720	4.2	0.2	8.3×10^4	2.7×10^2
Fused Silica (vitreous)	1.7×10^8	135	4.1	3.2	4.2×10^5	4.0×10^2
	8.9×10^7	150	4.0	2.8	3.7×10^5	2.4×10^2
	4.6×10^7	220	4.0	1.4	2.5×10^5	1.8×10^2
	2.2×10^7	300	4.0	0.6	1.9×10^5	1.2×10^2

5. Conclusions

Data obtained from impact fracture of brittle materials can be correlated with a linear lognormal particle size distribution and with a nearly constant brittle-fracture surface-energy factor. This methodology allows the total surface area of particles from impact fracture to be estimated. Reliable extrapolation of particle size distributions to any lognormal size range seems achievable. Confirmation of this methodology is under study.

II. TRANSPORT PROPERTIES OF NUCLEAR WASTE IN GEOLOGIC MEDIA

(M. G. Seitz, Jacqueline Williams,* N. Meldgin,†
P. Rickert,‡ S. M. Fried,‡ A. M. Friedman,‡ and
M. J. Steindler)

A. Introduction

Work during this quarter included porosity measurements of basalt columns by tritium elution, as well as batch tests to determine the effect of rubidium concentration on cesium adsorption by limestone.

Among the parameters which may greatly influence the migration behavior of a particular radionuclide in a particular rock are porosity, (the ratio of the volume of interstices of a granulated rock to the volume of its mass) along with trace-element concentration and the flow rate of groundwater. A number of porosity measurements are presented in this report. The rock used in current studies is Sentinel Gap basalt, and water simulating groundwater in a basalt is prepared from chemicals. Included here are a discussion of and data from two analytical techniques used to determine porosity. One technique is a simple gravimetric method in which entrapped air is displaced by water. For use of this method, the density of the particular material must be known or determined. This technique was used to measure porosity of granulated basalt in test tubes and in a steel column.

The second technique is a radiochemical procedure, involving elution of tritiated water through a column of granulated basalt. The tritium experiments were done at several different flow rates.

Batch partitioning experiments were performed with cesium on oolitic limestone, using synthetic groundwater solutions containing seven different concentrations of rubidium. Cesium adsorption is sensitive to cesium concentration in the solution and is likely to be sensitive to rubidium concentration in the solution as well. In nature, rubidium is about thirty times more abundant than cesium and may interact more with radiocesium during migration than does natural cesium. The solutions and rock materials were irradiated while adsorption took place to represent adsorption in a radiation field near solidified waste.

Also during this quarter, an experimental apparatus utilizing a Teflon sleeve was constructed that serves to confine a solid rock column in a fluid stream under high pressure. The apparatus and its use are described.

---

* Member of the Analytical Group of the Chemical Engineering Division.

† Mayfield Engineering Co., Chicago Ridge, IL.

‡ Chemistry Division.

B. Experimental

1. Porosity Determination From Densities

No readily available literature values were available of the densities of solid or 20-50 mesh basalt used as rock columns. Therefore, rapid and simple but reproducible measurements were made of (a) the bulk density of the granulated basalt and (b) the density of the granulated basalt exclusive of intergranular spaces. The basalt was pretreated by resieving the granulated basalt, removing fine material by washing, and then drying it.

a. Bulk Density of the Granulated Basalt

Round-bottom test tubes, used as surrogate columns, were weighed and partially filled with dry basalt, then reweighed to obtain the basalt weight. The tube was gently tapped several times on a smooth hard surface to tamp down the material, after which the basalt level was noted and marked. The content of the tube was dumped, and the tube was refilled to the same mark with water, then weighed to obtain the water weight. The density of the basalt was calculated by dividing the weight of basalt by its volume, which for these purposes is considered equal to the water volume. The results are shown in Tables 11 and 12.

Table 11. Bulk Density of Granulated Basalt Measured in 1.0-cm-ID Tubes

Basalt, g	H_2O, g	H_2O, cm^3	Density,[a] g/cm^3
10.86	7.65	7.66	1.42
10.77	7.57	7.58	1.42
11.52	8.41	8.43	1.37
9.96	7.00	7.01	1.42
6.87	4.93	4.94	1.39
10.40	7.35	7.36	1.41
9.7[illegible]	6.90	6.91	1.41
10.58	7.41	7.42	1.42

[a]Average basalt density for all measurements = 1.41 ± 0.02 g/cm^3.

b. Density of Sentinel Gap Basalt by Water Displacement

First, the specific gravity of distilled water under the experimental conditions was determined by weighing water in volumetric flasks. In each of two experiments, a commodious amount of basalt was then weighed in a clean dry volumetric flask, and the flask was then filled to the mark with water, any air bubbles were allowed to rise, and water was added if

Table 12. Bulk Density of Granulated Basalt Measured in 1.3-cm-ID Tubes

Basalt, g	No. of Taps	Amount of Water		Density,[a] g/cm^3
		g	cm^3	
10.26	10	7.20	7.21	1.42
9.35	10	6.80	6.81	1.37
10.69	20	7.33	7.34	1.46
10.65	20	7.66	7.68	1.39
8.67	10	6.01	6.02	1.44
8.69	10	6.01	6.02	1.44

[a]Average density for all measurements = 1.42 ± 0.03 g/cm^3.

necessary to bring the volume up to the mark. The flask and contents were reweighed to obtain the weight of water that had been displaced by basalt. The average of two results (which differed by 2 parts in 400) gave a density of 2.89 g/cm^3.

c. Porosity of Granulated Basalt

The porosity of granulated basalt, ε, can be determined from (1) the bulk density of granulated basalt, ρ_a, and (2) the density of the basalt exclusive of intergranular spaces, ρ_B, by the equation

$$\varepsilon = \frac{\rho_B - \rho_a}{\rho_B}$$

For the values of ρ_B and ρ_a given above, ε is calculated to be 0.51.

2. Porosity of Particulate Basalt Based on Intergranular Volume Measurements

A premeasured length of Type 316 stainless steel tubing equipped with Swagelok fittings and filled to capacity with a known weight of dry granulated basalt served as a rock column for both types of porosity measurements. For this measurement, a relatively large quantity of distilled water was pumped through the column at a moderate flow rate, after which the column containing wetted basalt was reweighed to obtain the weight of water which had displaced interstitial air in the column.

The intergranular porosity, approximated by the ratio of the volume of air displaced by water (equal to the volume of water) to the volume of basalt, was 0.42. This measurement was made once at the beginning of the infiltration experiments and will be repeated at a later time.

3. Porosity of Particulate Basalt Based on Elution of Tritiated Water

The tritium data were obtained using apparatus [SEITZ-1979A, Fig. 7] in which tritiated water is injected into a column of basalt at several known flow rates. Small fractions (5-drop) of the eluate are collected, and portions are measured for tritium activity using a liquid scintillation spectrometer.

The porosity of a column is approximated by solving the equation

$$\varepsilon = \frac{V_t}{V_{cc}}$$

where

ε = porosity of the columnar particles

V_t = volume of eluate corresponding to the fraction having the greatest observed tritium activity per unit volume (peak volume)

V_{cc} = volume of the column, as calculated from its dimensions.

Experimental results are given in Table 13. The porosity values given in Table 13 include corrections (~1% corrections) for the volume in the Tygon and stainless steel tubing used to connect the exit end of the column to the fraction collector.

Additional work with a granulated basalt column indicates that substantial amounts of air can be trapped within the column during infiltration with water. This is probably the cause of the variation in measured porosity values given in Table 13 and Section B.2 above. Air remaining within the column is expected to lower the apparent porosity so that the porosity measured by infiltrating columns with a solution can be considered the lower limit of the actual porosity.

These measured values are all lower than the 0.51 value measured in glass apparatus in which the total exclusion of air from the intergranular spaces was verified by visual observation. Therefore 0.51 is considered the best measure of the porosity of the granulated basalt in the columns.

C. Cesium and Rubidium Adsorption by Limestone in a Radiation Field

Batch partitioning experiments were performed to determine cesium adsorption on oolitic limestone, using synthetic groundwater solutions containing seven different concentrations of rubidium. The experiments were performed like other batch experiments [SEITZ-1979B, STEINDLER-1979B] and are described as follows.

Table 13. Porosity of 20-50 Mesh Sentinel Gap Basalt Based on Tritiated Water Elution

Expt. No.	Flow Rate, mL/min	Peak Range Vol, mL	Average Peak Vol, mL	Porosity,[a] fraction
148-111	0.192	2.89 2.97	2.93	0.375
148-119	0.289	3.26 3.46	3.36	0.430
148-121	0.176	2.02 2.13	2.08	0.264
148-123	0.0792	2.03 2.15	2.09	0.266
164-14[b]	0.326	3.50 3.77	3.63	0.403
164-22[b]	0.0985	3.42 3.68	3.55	0.392

[a]Porosity is calculated on the basis of the volume of the column being 7.76 cm^3.

[b]The eluant consisted of synthetic basalt groundwater which was 10^{-4}M in CsCl. No cesium was added in the other four runs.

At the start of each experiment, 3.0 g of limestone in a 15-mL polystyrene centrifuge tube was rinsed three times with one of the seven synthetic groundwaters containing stable rubidium. To promote the reaction of the synthetic groundwater solution with rock material, each tube was rotated end-over-end--both during rinsing and during the experiments to exchange radioactive rubidium and cesium.

During exchange of the radioactive species, one set of test tubes was irradiated in a ^{60}Co gamma field. The other set of tubes, placed outside the radiation field, served as controls. For both irradiated and nonirradiated samples, adsorption proceeded for sixteen days. The test tubes remained still and in the same laboratory environment (no ^{60}Co radiation field) for 3-5 h before individual 5-mL aliquots were filtered through 0.4 μm-pore Gelman membranes. Gamma detection for rubidium and cesium in these solutions was done later.

The dose rates at 15 points occupied by the test tube rack were measured from changes in absorbance of cobalt glass dosimeters at a light wavelength of 450 nm. Radiation doses varied in the area of the test tube rack (from 2.0 x 10^5 to 3.4 x 10^5 rads/h). Differences in dose rates at the locations specified in Fig. 12 are listed in Table 14. An average dose for the samples was taken to be the amount received at the central point of the middle radial plant, B center ($\sim$2.6 x 10^5 rads/h). This dose may be related to the radiation surrounding a waste canister as being equivalent to: (1) The dose accumulated in one year at a distance of one foot from the center of a canister (originally 5000 W) containing ten-year-old waste. (2) The dose

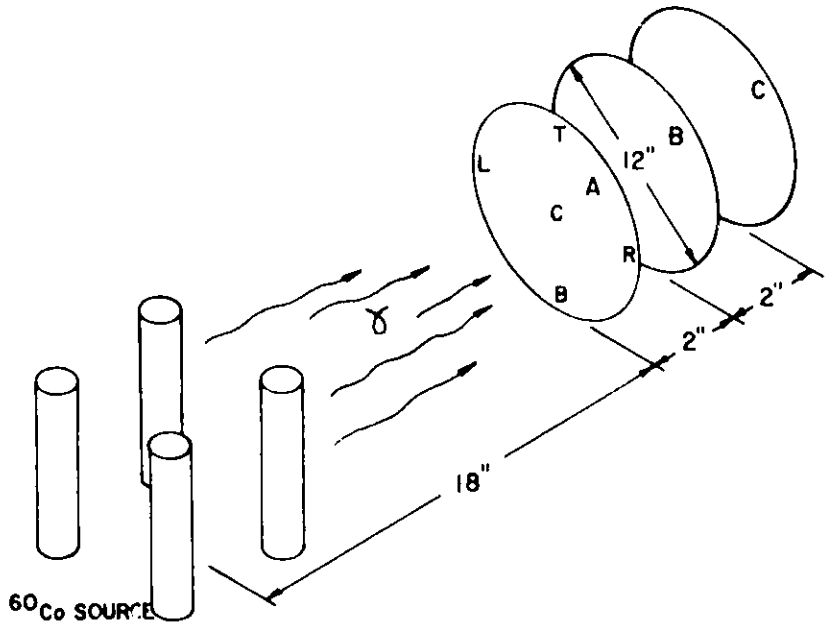

Fig. 7. Schematic Diagram used in Identifving Locations on a Test Tube Rack in a Radiation Field. Positions are: Top(T), Bottom(B), Right(R), Left(L), Center(C). Planes are: (A), (B), (C)

Table 14. Dose Rates at Locations Specified in Fig. 7

Dosimeter Location		Measured Dose Rate, rads/h
Plane	Position	
A	Top	3.0×10^5
A	Center	3.4×10^5
A	Bottom	3.4×10^5
A	Left	3.0×10^5
A	Right	3.0×10^5
B	Top	2.35×10^5
B	Center	2.65×10^5
B	Bottom	2.6×10^5
B	Left	2.4×10^5
B	Right	2.4×10^5
C	Top	2.0×10^5
C	Center	2.1×10^5
C	Bottom	2.0×10^5
C	Left	1.95×10^5
C	Right	1.95×10^5

accumulated in ten years at a distance 1.4 ft from the center of a canister (originally 5000 W) containing ten-year-old waste. Waste canisters have an inside diameter of 6 in., a steel wall thickness of 0.25 in., and a height of 8 ft [BLOMEKE].

The partition results obtained by radiochemically counting the solutions are given in Table 15. Partition coefficients for cesium and rubidium are generally lower in the irradiated sample experiments than in the nonirradiated sample experiments. However, the differences may not be a result of gamma radiation, but rather a result of differences in the temperatures of the two test tube racks. The nonirradiated samples were at 22°C to 24°C. The irradiated samples had a temperature of 29 to 32°C (30°C avg.). Dependence of cesium partition coefficient on temperature was observed by Couture and Seitz [COUTURE, SEITZ-1978]. In those experiments, kaolinite was found to possess a high affinity for cesium over sodium, which affinity diminished by two orders of magnitude between 25°C and 170°C. [EICHHOLZ] has also shown the dependence of cesium partition coefficient on temperature in batch experiments with both kaolin and shale and showed how this effect interferred with interpretation of radiation-effect experiments. Eichholz found that under conditions of increasing temperature, the partition coefficients for cesium decrease in the presence of kaolin but increase in the presence of shale.

Figure 8 relates cesium partition coefficients measured in the presence of cesium to cesium partition coefficients measured in the presence of rubidium. From Fig. 8, varying the amount of rubidium in solution can be seen to have the same large effect on cesium adsorption as varying the amount of cesium in solution.

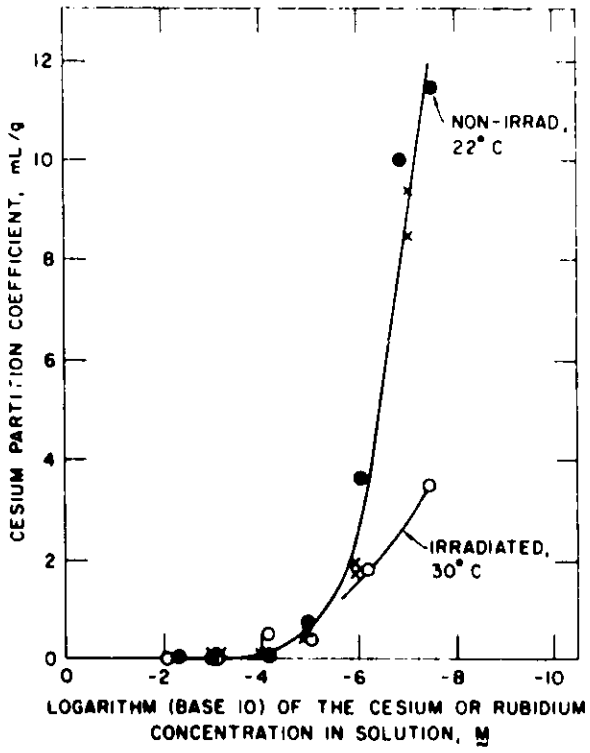

Fig. 8.

Cesium Partition Coefficients for Several Concentrations of Cesium or Rubidium. Crosses (x) are data for the various concentrations of cesium in solution, 7 and 8 days contact time, with a temperature of ∿22°C. Solid circles (●) are data with various concentrations of rubidium in solution, 16 days contact, and a temperature of ∿22°C. Open circles (o) are data with various concentrations of rubidium in solution, 16 days contact, a temperature of 30°C, and an irradiation field of ∿2.6 x 10^5 rad/h.

Table 15. Partition Coefficients for Rubidium and Cesium from Batch Tests with Irradiated and Nonirradiated Samples

Rb, Initial Wash Solution, M	Cesium				Rubidium			
	Irradiated Sample K_d Values		Nonirradiated Sample K_d Values		Irradiated Sample K_d Values		Nonirradiated Sample K_d Values	
	mL/g	Average	mL/g	Average	mL/g	Average	mL/g	Average
4.1×10^{-8}[a]	3.4		11.4		2.0		4.9	
	3.7		11.5		2.2		4.9	
	3.4	3.54	11.7	12.5	2.0	2.1	5.1	5.0
1.52×10^{-7}[a]	3.6		9.9		2.1		4.6	
	3.6		9.7		2.1		4.4	
	3.7		10.4	10.	2.3	2.2	4.6	4.5
8.4×10^{-7}	1.7		3.8		1.3		2.8	
	1.8		3.7		1.4		2.6	
	1.8	1.79	3.6	3.7	1.4	1.4	2.5	2.6
1.1×10^{-5}	0.3		0.59		-0.3		1.2	
	0.45		0.64		0.6		1.2	
	0.46	0.41	0.60	0.61	0.7	0.03	1.2	1.2
9.8×10^{-5}	0.63		0.84		0.002		0.3	
	0.69		0.08		0.07		0.3	
	0.69	0.67	0.08	8.3×10^{-2}	0.1	0.06	0.2	0.3

(Contd)

Table 15. (Contd)

Rb, Initial Wash Solution, M	Cesium				Rubidium			
	Irradiated Sample K_d Values		Nonirradiated Sample K_d Values		Irradiated Sample K_d Values		Nonirradiated Sample K_d Values	
	mL/g	Average	mL/g	Average	mL/g	Average	mL/g	Average
8.8×10^{-4}	0.00		0.007		0.0		-0.04	
	nd[b]		0.02		nd[b]		0.04	
	0.0001	∿0.0	0.008	0.01	0.0	∿0.0	-0.005	∿0.0
9.7×10^{-3}	0.006		0.003		0.0		0.07	
	0.002		0.005		0.0		0.1	
	0.007	∿0.0	0.005	0.004	0.0	∿0.0	0.08	0.09

[a]The rubidium concentrations of these solutions were below the detectable limits of atomic absorption spectrophotometry.

[b]The rubidium concentrations were calculated from the specific activity of the ^{86}Rb (6.9 mCi/mg at 12:00 a.m., August 23, 1979) and from pipetting solution, of known formulated rubidium concentrations.

nd indicates that the value was not determined because the test tube stopper leaked and solution was lost during irradiation.

D. Apparatus Development

An experimental apparatus was constructed to study the leach migration characteristics of radionuclides in rock cores. The apparatus is similar to previous experimental devices used to infiltrate rock in a fluid stream [SEITZ-1979C]. A change to using pressurized Teflon sleeve to hold a solid rock core is the major difference in equipment design (see Fig. 9). A diagram of the entire apparatus is shown in Fig. 10. Gases dissolved in solution will be regulated by use of a gas sparging apparatus described previously [SEITZ-1979A]. Minor problems are presently being corrected, and the apparatus should be available for experimentation shortly.

For the purpose of attaining higher confining pressures, the "O" rings initially used have been replaced with rubber Quad brand rings. The rings allow attainment of the greater pressure required to squeeze the Teflon cylinder tightly around the rock core in order to maintain aqueous flow through the rock rather than through a possible gap between the rock and the Teflon.

Teflon was chosen as the rock-holding medium because it is nonreactive with most aqueous solutions. The Teflon is, therefore, more desirable than the previously used adhesive sealant (*i.e.*, epoxy, [SEITZ-1979C]). Stainless steel (1/16-in.-OD) tubing has been incorporated into the apparatus to deliver fluid under high pressure to the outside of the Teflon sleeve.

High confining pressures are generated by using a No. 11100 Enerpac 0-10,000 psi hydraulic hand pump. Distilled water is used with this pump to pressurize the Teflon sleeve. With the currently used holder, the confining pressure upper limit occurs between 33 and 40 MPa (5000-6000 psi). In that range, the outer Quad Brand ring fails.

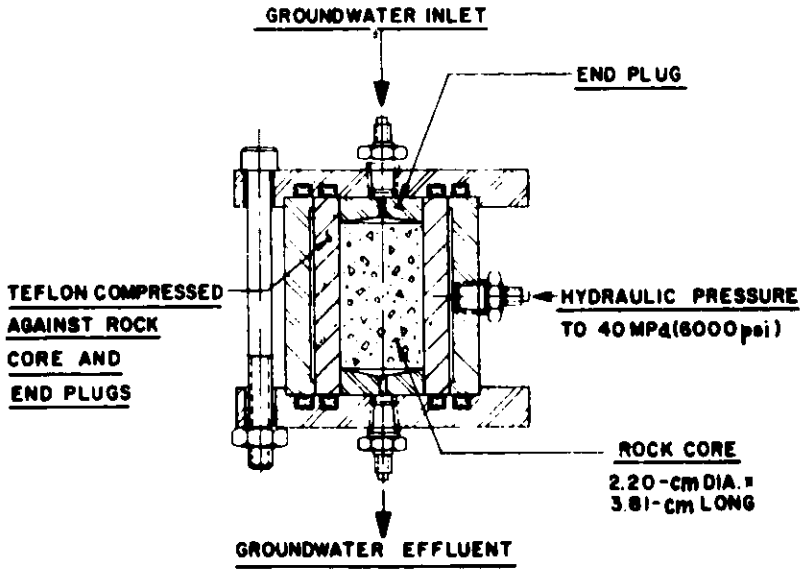

Fig. 9. Rock-Column Holder with Pressurized Teflon Jacket

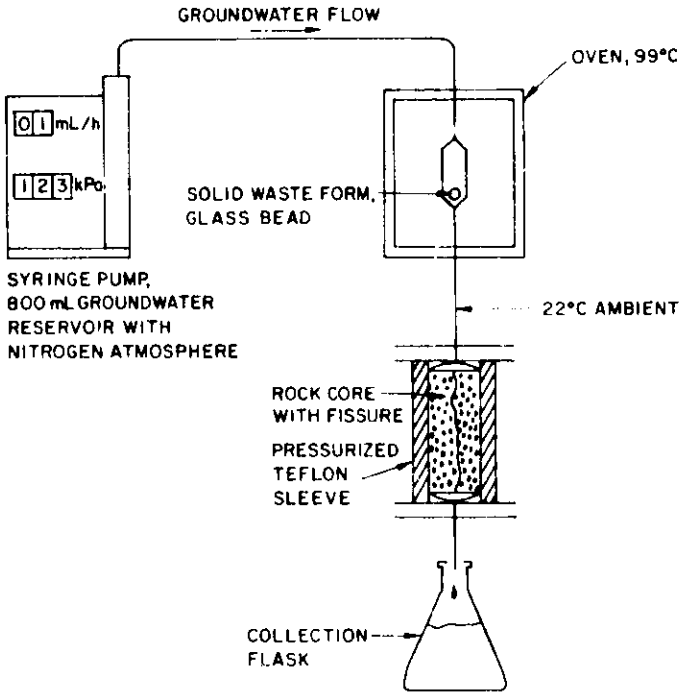

Fig. 10. Apparatus to be used in Leach-Migration Experiments with Solidified Waste Containing Plutonium, Americium, and Neptunium

An initial test of the Teflon sleeve was performed with 20.7-MPa (3000-psi) pressure maintained for one day on a Teflon sleeve containing a two-piece sandstone core. After removal of the core, it was observed that the Teflon sleeve had a ridge around its inner diameter at the level where the two core pieces met. On the basis that the Teflon flowed to fill the slight gap between the two pieces of sandstone, it appears that the Teflon sleeve will squeeze firmly around a rock core at 20.7 MPa.

To obtain a slow linear flow rate of the solution in the pores of the rock, the diameter of the core was increased from the 1.0-cm diameter originally used [SEITZ-1979C] to 2.20 cm. A larger cross-sectional area is required to maintain a low flow rate because the impermeable rocks (which require infiltration by high pressure) have little porosity subject to fluid flow.

To start an experiment, the solid waste container and the rock column (Fig. 10) are first connected to the metering pump, and then the pump and oven are turned on. The solution is collected in fractions until 0.2 to 5 L of solution has flowed through the rock. Experiments will be performed at flow rates of 0.1 mL/min and will last 7 to 35 days. Solution fractions will be taken using a fraction collector (~10 mL fraction) or will be taken manually (120- to 360-mL fraction). The eluate fraction will be analyzed for radioactivity. After termination of an experiment, the rock column may be sectioned and analyzed.

The amount of plutonium and americium leached from the solid waste form can be estimated from the leach rate of 2×10^{-5} g/cm^2·day at a temperature of 80°C [SEITZ-1978]. For glass formulated in the Brew (Model 1064-C) furnace and having plutonium and americium concentrations of 1.0 and 0.006 mg/g of glass, respectively, if a leach rate of 2×10^{-5} g/cm^2·day is assumed then 2.7×10^{-8} g of plutonium and 1.4×10^{-10} g of americium will be leached in every 145 mL of groundwater solution (one day's volume of solution, if one gram of glass is assumed to have a surface area of 1.27 cm^2). The activities of plutonium and americium leached per day at 80°C are 90 dps and 17 dps, respectively (using activities of plutonium and americium of 3.28×10^9 and 1.10×10^{11} dps/g, respectively).

In this manner, the adsorption of radionuclides by different rock cores may be studied and possibly results may be correlated with results of previous batch partitioning experiments. The rock materials chosen may be viewed either as the rock for siting a radioactive waste repository or as possible backfill material at a repository site. These experiments will yield needed information on radionuclide adsorption isotherms on rock.

III. TRACE-ELEMENT TRANSPORT IN LITHIC MATERIAL BY FLUID FLOW AT HIGH TEMPERATURE

(M. G. Seitz and R. A. Couture)

A. Introduction

This work covers two subjects: (1) the transport of Cs^+ ions through kaolinite columns and the associated experimental details and (2) sorption of iodate and other anions on ferric oxides and other substances. The cesium transport work consists mainly of an experiment (now proceeding) on the elution of Cs^+ by 0.100M $NaHCO_3$ at room temperature. That work is nearly complete, and the results should be ready for the next report.

We now have considerable experimental and theoretical information about anion exchange on ferric oxides; on this basis, we have considered methods for the disposal of radioactive iodine. Isotherms for sorption of iodate by Fe_2O_3 were reported previously [STEINDLER-1979B]. That work has now been extended to cover the iodate concentration range from 10^{-2} to 10^{-13}M, and we have measured sorption of iodate by sea sediments.

In order to explain the pH dependence and the shape of the isotherms, we have devised and tested three theories for the sorption of anions. These theories are applied here to the iodate data and to earlier data on the sorption of selenite ions [HINGSTON-1968].

Also, information is given on the iron content of kaolinite used in previous experiments to study the transport of dissolved iodine species through columns.

B. Theory: Anion Sorption on Oxides and Clay Minerals

1. pH Dependence

It was established previously that iodate is adsorbed by Fe_2O_3 more strongly in acid solution than in basic solution. The reason is easily seen qualitatively. The iron oxide surface consists mostly of -OH groups, which can hydrolyze to form $-O^-$ or $-OH_2^+$ [PARKS]. The surface density of $-OH_2^+$ and $-O^-$ is small. For example, the highest charge density on hematite recorded by [ATKINSON] was 4.9×10^{-4} μequiv cm^{-2} at pH 4 in 1M KCl. This corresponds to one -OH per 4.3 surface oxygen atoms, meaning that to a good approximation, the exhcange reaction can be represented by

$$-OH + IO_3^- = -OIO_2 + OH^- \qquad (1)$$

We expect IO_3^- to be mainly sorbed by its replacement of surface -OH groups and the formation of $Fe-OIO_2$ bonds. The pH effect is easily seen from Eq. 1. Reaction with $-OH_2^+$ sites, which have their greatest abundance at low pH, is represented by

$$-OH_2^+ + IO_3^- = -OIO_2 + H_2O \qquad (2)$$

Similarly, reaction with $-O^-$ sites is represented by

$$-O^- + IO_3^- + H_2O = -OIO_2 + 2OH^- \quad (3)$$

Reactions 2 and 3 show that the effect of pH on sorption should decrease somewhat at low pH, where $-OH_2^+$ populates a substantial portion of the surface, while the effect of pH should increase at high pH. At the pH of zero point of charge (8.5 to 9), the $-O^-$ and $-OH_2^+$ sites are equally abundant, and so reaction 1 should still hold. The equation for sorption of IO_4^- would show a similar pH effect.

However, sorption of an acid would show a much different pH effect. Consider HOI, which is a very weak acid, with a pK_a of 10, where K_a is the acid dissociation constant. One can write four equations, representing reactions of increasingly basic species and sites:

$$-OH_2^+ + HOI = -OI + H^+ + H_2O \quad (4)$$

$$-OH + HOI = -OI + H_2O \quad (5)$$

$$-O^- + HOI = -OI + OH^- \quad (6)$$

$$-O^- + OI^- + H_2O = -OI + 2OH^- \quad (7)$$

According to these equations, at low pH, increasing pH ought to increase the amount of sorption. At higher pH, however, as OH^- instead of H^+ begins to appear on the right-hand side of the equations, an increasing pH would decrease the amount of sorption. Thus, maximum sorption is expected at about the pH of zero point of charge of the oxide surface, represented by Eq. 5. This result differs from that of [HINGSTON-1967], who deduced that maximum sorption should occur at pH = pK_a.

2. Steric Hindrance and the Shape of the Isotherm

Equations 1 to 3 suggest that in principle, every accessible $-O^-$, $-OH$, or $-OH_2^+$ could be replaced, and that the entire surface could be covered with sorbed iodate. If this should be true, the exchange capacity would be nearly independent of pH and would be limited by the surface area, the size of the anions, and the way in which they are packed on the surface. The influence of steric hindrance on exchange capacity and on the functional form of the isotherm is considered in this section.

The shape of the isotherm is influenced by the requirement that if each anion sterically covers x sorption sites, a cluster of x free sites is needed for sorption. In this paragraph, we will derive the functional form of the isotherm. In the following paragraph, we will estimate the value of x for iodate sorption on Fe_2O_3. The rate of desorption can be expressed as

$$\frac{-d\Gamma}{dt} = k_r \, \Gamma/\kappa$$

where k_r = a constant, Γ = amount sorbed, and κ = anion sorption capacity. The fraction of surface not covered by sorbed anions is $1 - \Gamma/\kappa$, and the relative abundance of clusters of x free sites can be assumed to be $(1 - \Gamma/\kappa)^x$. Thus, the rate of adsorption is

$$\frac{d\Gamma}{dt} = k_f\ (1 - \Gamma/\kappa)^x c$$

where c = concentration of anions in solution and k_f is a constant. At equilibrium, the rates of sorption and desorption are equal, and so

$$\frac{\Gamma/\kappa}{(1 - \Gamma/\kappa)^x} = Kc \qquad (8)$$

where $K = k_f/k_r$.

It is possible to estimate the value of x in eq. 8 from geometric considerations. In solid iodates, the IO_3^- ion has a tetrahedral structure. The I atom occupies the vertex, allowing the oxygen atoms to pack more closely than they otherwise could. If one assumes that one oxygen atom in the IO_3^- ion replaces an O or OH on the oxide surface, there would be two oxygens and one I above the surface. The I atom is small enough that it might allow close-packing of the iodate oxygens above the surface. Thus, at saturation, iodate might be close-packed on the surface. This would mean that iodate could replace as much as 50% of the surface atoms if close-packed. (From the crystal structure of $NaIO_3$, the O-O distances in IO_3^- are 2.65 and 2.81 Å, while the I-O distances are 1.80 and 1.83 Å. At most, the I radius is $1.83 - \frac{2.65}{2} = 0.51$ Å, which is small enough for octahedral coordination and smaller than the radius of Fe^{3+} [0.64 Å]. If free to rotate, the IO_3^- ion would occupy as much surface area as 3.3 close-packed oxygen atoms and would cover an area occupied by part of seven oxygens atoms, Thus, we have three estimates for the iodate exchange capacity of Fe_2O_3: 1/7, 1/3.3, and 1/2 of the surface oxygens. Using a BET surface area value of 10 m^2/g (N_2 adsorption measurement performed by R. L. Malewicki of this Division), estimates for the exchange capacity of 3.0×10^{-5}, 6.4×10^{-5}, and 1.06×10^{-4} mol/g, respectively, were obtained. The first estimate agrees will with experimental values of 2.2×10^{-5} and 2.9×10^{-5} (Table 19 presented later in this report section).

There is another method of deriving an isotherm which is different from Eq. 8. It is mentioned here because it fits the iodate sorption data better than Eq. 8 does at high concentrations of iodate, although it fails at low concentrations. The exchange reaction can be written as a reaction between two end member components, as follows:

$$-OH + rIO_3^- = -(IO_3)_r(OH)_{1-r} + rOH^- \qquad (9)$$

The parameter r is the iodate exchange capacity, expressed as a fraction of the number of surface oxygen atoms, as deduced above, where $0 < r \leq 1$. If the activity of each component is equal to its mole fraction (ideal solution), the equilibrium constant, K, for reaction 9 is given by

$$K = \left(\frac{[OH^-]}{[IO_3^-]}\right)^r \frac{x_1}{x_2} \qquad (10)$$

where x_1 and x_2 = mole fractions of $-(IO_3)_r(OH)_{1-r}$ and $-OH$, respectively. Since $\Gamma = \kappa x_1$, where κ = iodate sorption capacity, assuming for the moment that $x_1 + x_2 = 1$, it follows from Eq. 10 that

$$\Gamma = \frac{\kappa K \left(\frac{[IO_3^-]}{[OH^-]} \right)^r}{1 + K \left(\frac{[IO_3^-]}{[OH^-]} \right)^r} \qquad (11)$$

Equation 11 predicts that even at the lowest IO_3^- concentrations, the amount sorbed is not proportional to the solution concentration. At very low iodate concentrations, at constant pH, $\Gamma \propto [IO_3^-]$, whereas Eq. 11 predicts that $\Gamma \propto [IO_3^-]^r$. If hydrolysis of the surface to form $-OH_2^+$ species is considered, the resulting equation is the same as Eq. 11 except that K becomes a function of pH, and so this conclusion is not altered.

C. Determination of the Iodate Sorption Isotherm at Trace Concentrations

1. Experimental Procedures

A nearly carrier-free iodate solution ($^{131}IO_3^-$) was prepared as follows: An $Na^{131}I$ solution (2 mCi in 2 μL of 0.1M NaOH) was obtained, 0.1 mL H_2O was added, and after 2 1/2 half-lives, an aliquot was treated with 3M HNO_3 + $NaNO_2$. I_2 was extracted with CCl_4, and the iodine was extracted back as IO_3^- into 5% NaClO. This last step required less than two minutes. "Hypochlorite oxidizes I^- to IO_3^- quantitatively at pH 5.5 to 7.0" [LAITENEN, p. 405]. Oxidation of I^- and subsequent extraction of I_2 was necessary to eliminate IO_4^- originally present.

Paper chromatography of the iodate solution according to procedures described in earlier reports revealed about 1.4% I^- and a trace of IO_4^- (probably less than 0.5%). The remainder was IO_3^-. Thin layer chromatography on a cellulose sorbent gave nearly identical results, but IO_4^-, was not found.

Quantities of 0-50 μL of this tracer solution were added to 4-mL aliquots of buffer solutions whose compositions are given in Table 16. Stable KIO_3 solutions were also added to some buffer solutions before the tracer was added. Final IO_3^- concentrations spanned seven orders of magnitude. The solutions were mixed, and weighed quantities of Fe_2O_3 were added. The glass test tubes were capped and rotated overnight. Then the mixtures were centrifuged, the clear solutions were analyzed for activity, and distribution coefficients were calculated. Blank experiments showed that no IO_3^- was sorbed by the test tubes.

The concentration of ^{131}I in the solutions was estimated by assuming a 75% efficiency for the NaI detector. The concentration of ^{127}I carrier was estimated from the $^{131}I/^{127}I$ ratio given by the supplier. The results are quite insensitive to large errors in these estimates, since they apply only to the linear part of the isotherm.

Two of the solutions were checked by paper chromatography after the experiments. All of the iodine was present at IO_3^-. No I^- or IO_4^- was found, although in one sample, 4.0% I^- or IO_4^- would be detectable at the 95% confidence level. Therefore, the results are considered very reliable.

Table 16. Compositions of Buffer Solutions

pH	Composition	
3.93	50 g	0.1M CH_3COOH
	8.9 g	0.1M CH_3COONa
5.74	2.8 g	0.1M CH_3COOH
	50 g	0.1M CH_3COONa

2. Results

The results are shown in Table 17 and Fig. 11. The results from the titrations reported in previous reports are also shown. The exchange capacity is assumed to be one-seventh of the oxygen atoms on the surface, assuming a surface area of 10 m^2/g. The rationale is that each IO_3^-, if free to rotate, will sweep over the space occupied by seven oxygen atoms.

Table 17. Isotherm for Adsorption of Iodate by Fe_2O_3, Showing Probable Errors.[a] K_d = distribution coefficient

pH	$[IO_3^-]$, M	Amount Sorbed, mol/g	K_d, L/kg
3.86	$(5.7 \pm 0.9) \times 10^{-14}$	$(1.66 \pm 0.007) \times 10^{-14}$	290 ± 45
	$(5.07 \pm 0.16) \times 10^{-13}$	$(1.69 \pm 0.002) \times 10^{-13}$	333 ± 12
	$(2.06 \pm 0.01) \times 10^{-11}$	$(6.96 \pm 0.001) \times 10^{-12}$	340 ± 9
	$(2.08 \pm 0.01) \times 10^{-11}$	$(6.96 \pm 0.001) \times 10^{-12}$	335 ± 9
	$(1.15 \pm 0.03) \times 10^{-8}$	$(3.09 \pm 0.004) \times 10^{-9}$	269 ± 9
	$(1.24 \pm 0.03) \times 10^{-7}$	$(3.15 \pm 0.004) \times 10^{-8}$	254 ± 8
	$(1.29 \pm 0.03) \times 10^{-7}$	$(3.15 \pm 0.004) \times 10^{-8}$	244 ± 8
	$(2.03 \pm 0.04) \times 10^{-6}$	$(2.97 \pm 0.005) \times 10^{-7}$	146 ± 4
5.74	$(2.00 \pm 0.11) \times 10^{-13}$	$(1.48 \pm 0.012) \times 10^{-14}$	74 ± 4
	$(1.98 \pm 0.03) \times 10^{-12}$	$(1.49 \pm 0.004) \times 10^{-13}$	75 ± 2
	$(7.09 \pm 0.02) \times 10^{-11}$	$(6.29 \pm 0.003) \times 10^{-12}$	89 ± 1
	$(3.60 \pm 0.05) \times 10^{-8}$	$(2.75 \pm 0.007) \times 10^{-9}$	76 ± 2
	$(3.96 \pm 0.22) \times 10^{-7}$	$(2.79 \pm 0.03) \times 10^{-8}$	70 ± 4
	$(5.30 \pm 0.24) \times 10^{-6}$	$(2.52 \pm 0.033) \times 10^{-7}$	48 ± 2

[a] 50% confidence level, computed from counting statistics and precision of pipetting and weighing.

The results are considered very convincing that at low concentrations, the amount of iodate sorbed is proportional to the amount in solution. One should also note that the capacity appears to be independent of pH (the curves converge), in contrast to the belief of [HINGSTON-1967,-1968] that the capacity increases with decreasing pH.

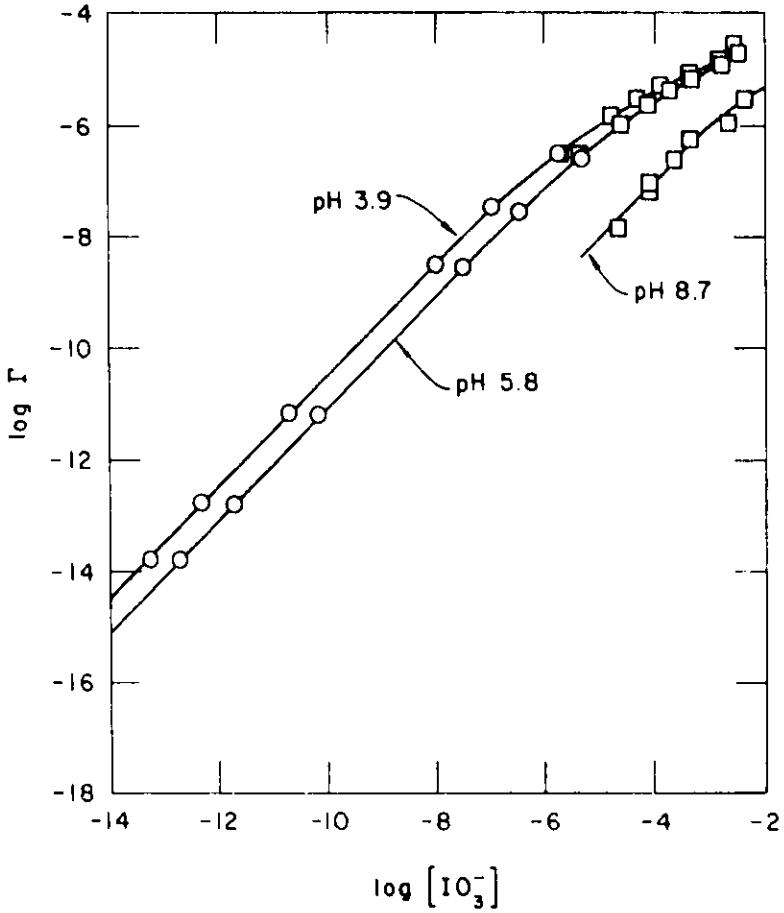

Fig. 11. Sorption of Iodate by Hematite (Fe_2O_3). Γ is amount sorbed, mol/g Fe_2O_3. $[IO_3^-]$ is in units of molarity. Squares indicate titrations, and circles indicate radiometric measurement. ANL Neg. No. 308-80-116

The change in standard free energy for the reaction

$$—Fe\text{-}OH + IO_3^- = —FeIO_3 + OH^-$$

is estimated to be 8 kcal/mol from the data obtained at pH 5.74.

D. Sorption of Iodate by Pelagic Red Clay and Hematite from Seawater

1. Experimental Procedures

Because of the possibility that iodine-129 will be disposed of in sea sediments, the sorptive behavior of red clay and hematite in seawater was investigated. Two samples of Pacific pelagic red clay, taken by the Deep Sea Disposal Project, were obtained. These owe their brown color ("red clay" is actually brown) to free iron oxides. Total Fe_2O_3 in the two samples was 4.3% and 4.7%. Weighed samples of hematite and subsamples of the red clay were added to two types of solutions along with their contained seawater. The first was artificial seawater; the second was artificial

seawater except that bicarbonate was omitted and 6.06 g/L Trizma base and 0.045 mol/L HCl were added. Both solutions were filtered through 0.45-μm Millipore filters before use. Known quantities of KIO_3 solution were added to all samples, which were rotated overnight in sealed test tubes. (Some of the samples were dispersed ultrasonically before the addition of KIO_3.) After equilibration, the test tubes were centrifuged, and the supernatant solutions were titrated to measure iodate.

2. Results

The results are shown in Table 18. Experiment 2 used a higher solid/solution ratio than experiment 1, and so the results of experiment 2 are more accurate. It is clear that significant amounts of iodate were adsorbed from seawater. Unfortunately, the pH of the hematite-containing samples dropped low enough to make direct comparison with the sea sediments difficult. However, comparison with previous results suggests that (1) sea salt does not decrease sorption appreciably in comparison to 0.1M $NaClO_4$ at the same pH, and (2) sample LL44-GPC2 sorbs about one-tenth as much iodate as the hematite does. Since iron oxide constitutes less than 10% of the sediment sample, it appears to sorb more than reagent grade hematite. It probably has a greater specific surface area than the hematite has.

Table 18. Sorption of Iodate by Red Clay and Hematite in Seawater and Modified Seawater

Exp. Number	Sample	Solution	Final pH	Iodate Sorbed, mol/g dry weight	Final $[IO_3^-]$ M
1	LL44-GPC2	(artificial seawater)	7.56	9×10^{-9}	2.2×10^{-5}
				2×10^{-7}	2.1×10^{-4}
				7×10^{-8}	4.5×10^{-4}
				5×10^{-7}	2.25×10^{-3}
				2×10^{-7}	4.54×10^{-3}
1	LL44-GPC2	(seawater with Trizma and HCL)	7.36	$\leq 2 \times 10^{-8}$	2.3×10^{-5}
				2.7×10^{-7}	2.2×10^{-4}
				2.8×10^{-7}	8.9×10^{-4}
				2×10^{-6}	4.2×10^{-3}
2	LL44-GPC2	(seawater with Trizma)	7.37	3.6×10^{-7}	2.2×10^{-4}
		(seawater)	7.6	3.3×10^{-7}	2.5×10^{-4}
2	Core 11	(seawater with Trizma)	7.25	1.6×10^{-7}	1.5×10^{-4}
		(seawater)	7.68	2.2×10^{-7}	1.5×10^{-4}
2	Hematite	(seawater with Trizma)	5.92	2.0×10^{-6}	6.2×10^{-5}
		(seawater)	4.46	2.0×10^{-6}	5.4×10^{-5}

E. Sorption of HOI by Kaolinite or Aluminum Oxide

In previous quarterly reports, it was reported that iodine-131 appeared to be bound to kaolinite in 0.1M $NaHCO_3$ at the end of a column experiment. The clay was analyzed for iodine-131, and two peaks were found: one small peak for clay at the top of the column, associated with an Fe_2O_3 stain; and a large peak in the middle of the column, apparently not associated with Fe_2O_3.

Recently, an identical sample of kaolinite, which had not been used in a column, was analyzed by Mössbauer spectroscopy for total iron and leachable iron, in order to determine the amount and nature of iron in the kaolinite. The kaolinite was found to contain 0.27% Fe_2O_3, of which 5% (<0.014%) is leachable by a Na citrate - Na dithionate solution, according to a standard test for free iron oxides. Mössbauer spectroscopy (analytical work and interpretation by Gopal Shenoy*) revealed no hematite and probably no FeOOH (goethite) in the kaolinite. Accordingly, the iron is considered to be substituted for aluminum in the kaolinite lattice.

These results support the contention that iodine-131 was not bound to an iron oxide impurity, but bound to the kaolinite itself. The only other phase likely to be present is a hydrous oxide of aluminum, which could form in trace quantities by leaching of the kaolinite during the experiment.

Which species of iodine could be bound to kaolinite? In previous experiments, IO_3^-, I^-, and I_2 were ruled out. That leaves IO_4^- and HOI. In Section B.1 above it was deduced that IO_4^- sorption ought to be lowest in alkaline solutions, while HOI sorption ought to be at a maximum at the pH of zero point of charge (ZPC). For Al_2O_3, the reported ZPC values are 7 to 9.5, and the ZPC of kaolinite is reportedly about 7.3. IO_3^- is thought to be sorbed by oxides and hydrous oxides of aluminum under acid conditions, and so the oxyanions of aluminum apparently do bond to aluminum ions. This suggests that (1) IO_3^- and/or IO_4^- was sorbed by small amounts of hydrous aluminum oxide in the column or (2) HOI is strongly sorbed by kaolinite and/or hydrous oxides of aluminum in neutral and slightly alkaline solutions. As noted in previous reports, an attempt to prepare HOI to test this hypothesis failed.

F. Sorption of Iodate and Selenite from Solutions - Test of the Models

Equation 8 was tested with data (obtained from a plot) by [HINGSTON-1968] on sorption of selenite ions by FeOOH (goethite). Figure 12 shows a plot of $\log (1 - \Gamma/\kappa)$ *versus* $\log \Gamma/\kappa - \log c$. The straight line plots indicate that the data fit Eq. 8 very well, with a slope, 1/x of 1/5. The assumption of slightly different sorption capacities leads to somewhat different slopes: good fits could also be obtained with slopes ranging from 1/4 to 1/7. However, it does appear that a slope of 1, which corresponds to the Langmuir isotherm, does not give a satisfactory fit of the data. We conclude that the data are consistent with Eq. 8, which indicates that sorption of selenite ions (SeO_3^{2-} or $HSeO_3^-$) probably does occur by replacement of surface $-O^-$ and $-OH$ groups, and that each sorbed ion sterically covers more than one sorption site.

---

*Solid State Science Division, Argonne National Laboratory.

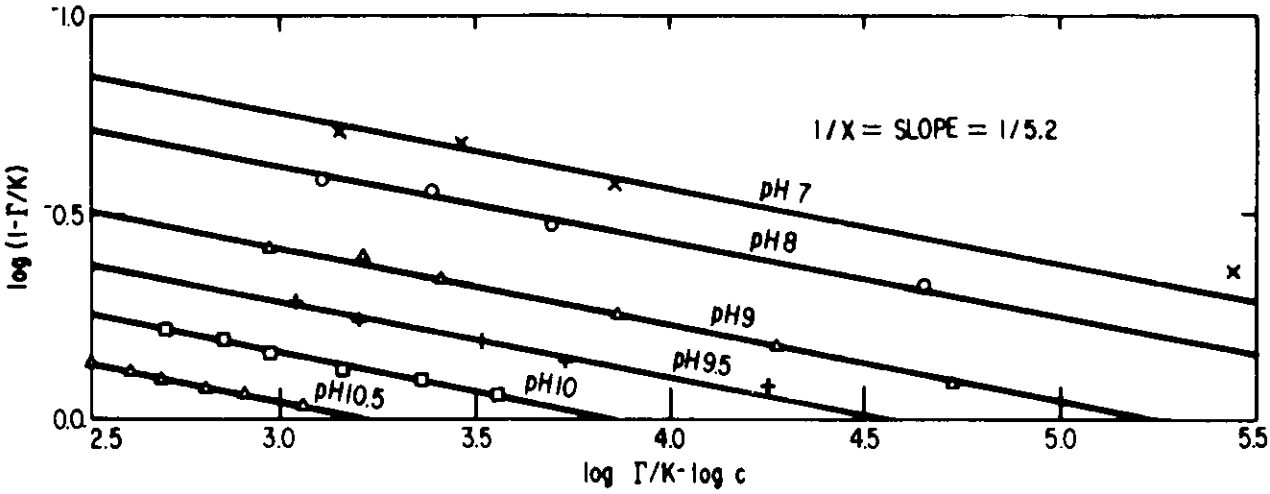

Fig. 12. Selenite Sorption by FeOOH. Data fitted to the logarithmic form of Eq. 8: $\log \Gamma/\kappa - \log c = x \log (1 - \Gamma/\kappa) + \log K\ (pH)$, with $\kappa = 115$ μmol/g.

However, Eq. 8 apparently does not adequately fit the iodate data. If the parameters of Eq. 8 are adjusted to represent sorption at intermediate solution concentrations, then Eq. 8 predicts sorbed concentrations which are much lower than observed at low and high iodate concentrations. There are at least two possible reasons. First, there may be an appreciable amount of IO_3^- found electrostatically in the interlayer region of the liquid phase, in addition to the IO_3^- replacing hydroxyl groups on the surface. Second, there may be more than one type of sorption site, each with its own equilibrium constant. For example, George Parks of Stanford University (oral communication) has pointed out that the Fe_2O_3 contains sulfate impurities (about 0.05%) which may leach out and create vacancies in the lattice which bind iodate relatively strongly.

Equation 11 does fit the iodate sorption data rather well at intermediate and high concentrations, as Table 19 shows. However, it fails completely at low concentrations.

Possibly, steric hindrance also plays a substantial role in cation sorption. [WAHLBERG-1962,-1965] found that partitioning coefficient of Sr^{2+} and Cs^+ between clay minerals and solutions does not obey a linear inverse relation with the concentration of the competing cation--that is, by analogy with anion sorption, $r < 1$.

G. Disposal of Iodine-129

Pelagic red clay sorbs iodate in seawater. It also has dissolved oxygen in the interstitial water [GRUNDMANIS], so IO_3^- is probably stable in the interstitial water. Red clay is probably a suitable burial medium because it is rather impermeable and the seawater above pelagic red clay deposits has enormous dilution capacity. Also, as Table 18 suggests, even in seawater at pH values of 7.5-7.7, an appreciable fraction of iodate might be sorbed by sediment, giving an additional safety factor. Unknowns at this point are the *in-situ* pH in pelagic clay and the effects of temperature and competition from silicate and phosphate.

Table 19. Sorption of Iodate by Hematite

pH 3.86	r = 0.75
$K = 3.5 \times 10^{-9}$	κ = 21.8 μmol/g

	Γ, μmol/g Fe_2O_3	
$[IO_3^-]$, μM	Calculated	Observed
2.5	0.28	0.28
16	1.08	1.07
52	2.45	2.55
141	4.60	4.63
396	8.01	7.53
1422	13.13	13.3

pH 5.77	r = 0.74
$K = 7.1 \times 10^{-8}$	κ = 28.7 μmol/g

	Γ, μmol/g Fe_2O_3	
$[IO_3^-]$, μM	Calculated	Observed
4.4	0.27	0.27
25.2	0.95	0.95
79.5	2.14	2.18
199	3.93	3.83
466	6.60	6.60
480	6.71	6.40
1530	12.0	11.9
3420	16.3	18.7

There is one promising alternative. It is well known that organic matter sorbs I^- [WHITEHEAD]. Charcoal ground to 80-200 mesh is reported to have distribution coefficients for I^- of >60 L/kg at all values of pH below 9 and >1000 L/kg below pH 5 [IKEDA]. It would be interesting to test the sorptive properties of coal for possible use in iodine-129 disposal.

REFERENCES

Atkinson

R. J. Atkinson, A. M. Posner, and J. P. Quirk, *Adsorption of Potential-Determining Ions at the Ferric Oxide-Aqueous Electrolyte Interface*, J. Phys. Chem. *71*, 550-558 (1967).

Axelson

J. W. Axelson and E. L. Piret, *The Crushing of Single Particles of Crystalline Quartz*, Ind. Eng. Chem. *42*, 665 (1950).

Blomeke

J. O. Blomeke, E. Sander, J. P. Nichols, S. Lindenbaum, R. S. Dillon, E. D. Arnold, and H. F. Soard, *An Analysis of Energy Storage and Its Effects on the Proposed National Radioactive Waste Repository*, Report ORNL-TM-3403 Oak Ridge National Laboratory (1971).

Bonnell

P. H. Bonnell, *Fines Analysis of Plutonium Dioxide Microspheres After Impact*, Mound Laboratory Report MLM-1626 (1969).

Couture

R. A. Couture, M. G. Seitz, and M. J. Steindler, *Experimental Trace-Element Transport by Fluid Flow at Elevated Temperatures: Ion Exchange on Kaolinite*, Am. Geophys. Union Trans. *59*, 1225 (1978).

Eichholz

G. G. Eichholz, T. F. Craft, B. G. Wahlig, P. D. Simpson, M. D. Mathenz, E. B. Shingelton, K. A. Will, and R. J. Titolo, *Subsurface Migration of Radionuclide Waste Materials by Particulate Transport*, Annual Report for The Office of Nuclear Waste Isolation, for period September 1, 1978 to August 31, 1979, Georgia Institute of Technology, Atlanta, GA (1979).

Flynn

K. F. Flynn, L. J. Jardine, and M. J. Steindler, *Method for Determining Leach Rates of Simulated Radioactive Waste Forms*, American Chemical Society Symposium on Radioactive Waste in Geologic Storage, ACS Symposium Series *100*, 115 (1979).

Grundmanis

V. Grundmanis and J. W. Murray, *Oxygen Profiles and Aerobic Respiration in Equatorial Pacific Sediments*, *Am. Geophys. Union Trans. 59*, 1118 (1978).

Herdan

G. Herdan, *Small Particle Statistics*, Academic Press, London (1960).

Hingston-1967

F. J. Hingston, R. J. Atkinson, A. M. Posner, and J. P. Quirk, *Specific Adsorption of Anions*, Nature *215*, 1459-1461 (1967).

Hingston-1968

F. J. Hingston, A. M. Posner, and J. P. Quirk, *Adsorption of Selenite by Goethite*, Adv. Chem. *79*, 82-90 (1968).

Ikeda

Nagao Ikeda and Kiriko Tanaka, *Column Chromatographic Separation of Radioactive Tellurate, Tellurite, Iodide, and Iodate by Active Charcoal*, J. Chromatogr. *114*, 389-395 (1975).

Kenny

W. J. Kenny and E. L. Piret, *Slow Compression Crushing of Single Particles of Glass*, AIChE J. *7*, 199 (1961).

Laitenen

H. A. Laitenen, *Chemical Analysis*, McGraw-Hill (1960).

McElroy-1977

J. L. McElroy, *Quarterly Progress Report Research and Development Activities*, Waste Fixation Program, October-December 1976, Battelle Pacific Northwest Laboratories Report, PNL-2264 (November 1977).

Mecham-1980A

W. J. Mecham, L. J. Jardine, and M. J. Steindler, *The Lognormal Equation of the Particulate State of Matter as Derived from Brittle-Fracture Mechanics*, to be presented at American Association for the Advancement of Science, Annual Meeting, at San Francisco, California, January 3-8, 1980.

Mecham-1980B

W. J. Mecham, L. J. Jardine, and M. J. Steindler, *The Effect of Impact Energy on Solid-Waste Composites of Brittle and Ductile Materials*, Proceedings of the International Symposium on Ceramics in Nuclear Waste Management, April 30-May 2, 1979, Cincinnati, Ohio; to be published by the American Ceramic Society.

Parks

G. A. Parks and P. L. de Bruyn, *The Zero Point of Charge of Oxides*, J. Phys. Chem. *66*, 967-973 (1962).

Seitz-1978

M. G. Seitz and R. Couture, *Transport in Lithic Material by Fluid Flow at High Temperatures, Quarterly Report, July-September 1978*, Argonne National Laboratory Report ANL-79-6.

Seitz-1979A

M. G. Seitz, P. G. Rickert, S. M. Fried, A. M. Friedman, and M. J. Steindler, *Studies of Nuclear-Waste Migration in Geologic Media, Annual Report October 1977-September 1978*, Argonne National Laboratory Report ANL-79-30 (1979).

Seitz-1979B

M. G. Seitz, P. G. Rickert, R. Couture, J. Williams, L. Meldgin, S. M. Fried, A. M. Friedman, and M. J. Steindler, *Transport of Radionuclides in Geologic Media*, Annual Report for the Waste Isolation Safety Assessment Program, for period October 1, 1978 to September 30, 1979, R. Serne, Chairman.

Seitz-1979C
M. G. Seitz, R. A. Courture, and M. J. Steindler, *Leach-Migration Experiments to Determine the Mobility of Radionuclides in Geologic Media*, Trans. Am. Nucl. Soc. *32*, 385, 386 (1979).

Steindler-1979A
M. J. Steindler *et al.*, *Chemical Engineering Division Fuel Cycle Programs, Quarterly Progress Report, January-March 1979*, Argonne National Laboratory Report ANL-79-45.

Steindler-1979B
M. J. Steindler *et al.*, *Chemical Engineering Division Fuel Cycle Programs Quarterly Progress Report, April-June 1979*, Argonne National Laboratory Report ANL-79-99.

Wahlberg-1962
J. S. Wahlberg and M. J. Fishman, *Adsorption of Cesium on Clay Minerals*, U. S. Geol. Surv. Bull. 1140-A, 30 pp. (1962).

Wahlberg-1965
J. S. Wahlberg, J. H. Baker, R. W. Vernon, and R. S. Dewar, *Exchange Adsorption of Strontium on Clay Minerals*, U. S. Geol. Surv. Bull. 1140-C, 26 pp. (1965).

Wallace
R. M. Wallace and J. A. Kelley, *An Impact Test for Solid Waste Forms*, Savannah River Laboratory Report DP-1400 (1976).

Whitehead
D. C. Whitehead, *The Sorption of Iodide by Soil Components*, J. Sci. Food Agri. *25*, 73-79 (1974).

Zeleny
R. A. Zeleny and E. L. Piret, *Dissipation of Energy in Single-Particle Crushing*, Ind. Eng. Chem. Process Des. Dev. *1*, 37-41 (1962).